Discover Environment

RESEARCH Open Access

Flood susceptibility prioritization in Dimoria block Assam using GIS and analytical hierarchy process

Sahil Choudhury[1,2*] and Mala Dutta[1]

*Correspondence:
choudhurysahil68@gmail.com

[1] Department of Geography, Faculty of Earth Sciences, Cotton University, Guwahati, Assam, India
[2] Department of Geography, Pandu College, Guwahati, Assam, India

Abstract

Assam is highly susceptible to frequent flooding, which significantly affects socio-economic conditions. Despite the widespread application of Geographic Information System (GIS) based Analytical Hierarchy Process (AHP) models for flood susceptibility assessment, there remains a lack of micro-spatial analyses focused on semi-urban and rural fringe regions such as Dimoria Block. Existing regional-scale assessments often overlook local variations in topography, land cover, and hydrological conditions, limiting their applicability for site-specific planning. The present study integrates GIS and AHP to delineate flood susceptibility zones in Dimoria Block using eleven flood-conditioning parameters. Multicollinearity analysis was conducted, followed by weighted overlay and sensitivity analyses. Rainfall and land use/land cover (LULC) emerged as the most influential factors. The results indicate that 54.75% of the study area falls within the high flood susceptibility zone, 36.72% within the moderate zone, and 8.52% within the low zone. The final flood susceptibility map was validated using both quantitative and qualitative approaches. The receiver operating characteristic (ROC) analysis yielded an area under the curve (AUC) value of 0.936, indicating high predictive accuracy. Validation using field surveys and official flood records further supports the robustness of the model. This study presents a localized flood susceptibility assessment framework for Dimoria Block and demonstrates the applicability of GIS–AHP approaches in data-scarce environments. The findings provide useful inputs for flood mitigation planning, land-use management, and disaster risk reduction strategies at the local level.

Keywords: Flood, Dimoria, GIS, Weighted overlay, AHP

1 Introduction

Floods are among the world's most significant natural hazards, occurring due to intense rainfall, snowmelt, or inadequate drainage systems that are unable to accommodate excess surface runoff [1]. Their impacts are exacerbated by population growth, unplanned land-use change, land degradation, and climate change [2]. Globally, floods have resulted in substantial displacement and loss of life [3], along with long-term socio-economic impacts [4]. Between 2000 and 2019, flood events affected over 1.65 billion people, caused nearly 122,000 fatalities, and led to economic losses amounting to USD

563 billion [5]. In recent years (2023–2025), several extreme flood events have been reported in the Republic of Congo, Afghanistan, and Bangladesh, resulting in widespread displacement and damage associated with intense rainfall and inadequate infrastructure [6, 7].

Asia experiences flood events more frequently than any other continent [8], with monsoon-dominated countries such as India exhibiting particularly high levels of exposure [9]. India has recorded the highest number of flood-related fatalities in Asia [10] and has experienced several major flood events, including the Mumbai flood (2005), Bihar floods (2007–2008), Assam flood (2012), Uttarakhand flood (2013), Jammu and Kashmir flood (2014), and Kerala flood (2018) [11].

Assam is among the most flood-prone states in India [12, 13] and is located within the Brahmaputra basin, where monsoon rainfall contributes approximately 90% of the annual precipitation [14]. Variability in climatic conditions has contributed to increases in the intensity and frequency of flood events [15], resulting in recurrent impacts on settlements, agriculture, infrastructure, and livelihoods [16]. Historical flood occurrences in 1954, 1962, 1972, 1977, 1984, 1988, 1998, 2002, 2004, 2012, and 2017 highlight the long-standing flood susceptibility of the region [17]. Approximately 39.58% of Assam's geographical area (31,500 km^2) is classified as flood-prone [16], with an estimated 0.7–7 million people affected annually between 2010 and 2020; more than 4 million people were affected during the flood events of 2017, 2019, and 2022 [18].

Given the recurrent nature of flooding in the region, reliable flood assessment is essential for effective planning and risk management. Conventional post-event field surveys, although valuable, are often time-consuming, spatially constrained, and insufficient in resolution for detailed planning purposes [19–21]. Consequently, remote sensing (RS) and geographic information system (GIS) techniques have become essential tools for flood monitoring, facilitating rapid inundation mapping, spatial analysis, and multi-temporal assessment [22–25]. Furthermore, the integration of GIS with the Analytical Hierarchy Process (AHP) enables systematic evaluation of multiple flood-conditioning factors [26, 27]. AHP has been widely adopted in flood hazard studies due to its capability to incorporate expert judgment and prioritize criteria through structured pairwise comparisons [28–30], thereby supporting the assessment of parameters influencing flood susceptibility [31, 32].

Despite significant flood research in Assam, Dimoria Block remains understudied, even though it experiences recurring seasonal floods. In 2019, floods affected 40,000 people in Sonapur Circle, damaging embankments in Amara Pathar [33]. In May–June 2020, 40 villages were submerged, with Rewa Pathar and Durung Gaon among the worst impacted [34, 35]. In 2024, floods affected eight villages and 18 fisheries [36], while recurrent flash floods have contributed to increased sedimentation and reduced water-holding capacity of local waterbodies. Additionally, the Digaru and Kolong rivers continue to contribute to annual flooding in the region [37].

Under these conditions, Dimoria Block requires a detailed micro-spatial assessment of flood susceptibility. Accordingly, the present study integrates GIS and AHP techniques to delineate flood susceptibility zones using eleven hydro-geomorphic parameters. Although GIS–AHP frameworks have been applied in various regions of India and Assam, three key research gaps persist in the context of Dimoria Block: (i) the absence

of micro-spatial flood hazard assessment for this highly flood-prone area, (ii) the lack of a multi-criteria framework incorporating eleven hydro-geomorphic parameters simultaneously, and (iii) the absence of robust validation using both ROC–AUC analysis and village-level governmental flood records. The originality of this study lies in the integration of a GIS-based AHP approach with fine-scale spatial analysis to generate a detailed flood susceptibility zonation for Dimoria Block. By addressing these gaps, the study provides a localized, evidence-based framework to support disaster preparedness and land-use planning.

2 Review of literature

Increasing flood frequency and intensity associated with climate change and anthropogenic disturbances has increased the need for reliable flood susceptibility assessment frameworks. GIS–AHP systems are widely used for flood susceptibility mapping, disaster management planning, and resource optimization across diverse environments [38, 39]. The adaptability of AHP allows the integration of hydrological, topographic, land-use, and socio-economic variables, supporting its application in both arid [40] and urban environments [41]. A GIS-based hybrid of AHP and Frequency Ratio (FR) models has also been applied in regions such as the Jhelum–Chenab system, demonstrating how statistical approaches can complement MCDA techniques in assessing the influence of parameters such as drainage density [42]. Although such hybrid models exist, the present study focuses exclusively on an AHP-based framework.

In India, GIS–AHP approaches have been applied extensively across varied hydro-geomorphic contexts, including the Ganges–Brahmaputra Basin [43, 44] and the Western Ghats [45]. For example, [45] identified approximately 25% of the Western Ghat coastal belt as highly flood-prone using multi-source geospatial data and AHP; the model achieved an AUC value of 0.84, indicating satisfactory predictive performance. Assam's flood susceptibility has also been examined using GIS–AHP weighted overlay analysis [13, 46, 47]. Studies conducted in the Brahmaputra [44] and Kopili [14] basins have assessed rainfall deviation, drainage density, lithology, and land-use changes to map flood susceptibility. Micro-spatial analyses in Nagaon and Cachar districts indicate strong correspondence between AHP-based susceptibility maps and observed flood-impact data [46, 47].

The literature indicates a progression from broad-scale GIS–AHP applications toward more localized and data-driven flood modeling approaches. However, several challenges persist, including data limitations, model uncertainty, and dynamic influences such as land-use change and climate variability [38, 48]. Despite these limitations, AHP remains widely applied compared to other MCDA techniques (including TOPSIS, VIKOR, and Fuzzy-AHP) due to its methodological simplicity, transparency, and consistent performance in flood susceptibility studies [49, 50]. Recent research has explored hybrid MCDA–machine learning models to further enhance predictive accuracy and reduce uncertainty [51, 52].

In summary, while GIS–AHP frameworks have been applied at regional and district scales in Assam, Dimoria Block has received limited attention in terms of micro-level flood susceptibility assessment, despite documented flood impacts, underscoring the need for the present study's localized, multi-parameter approach.

3 The study area

The Dimoria CD Block is situated between 26°0′0″N to 26°10′14″N latitudes and 91°45′ 5″ E to 92°5′0″ E longitudes, respectively (Fig. 1). It is in the southeastern part of Kamrup (Metropolitan) district of Assam. Bordered by Meghalaya to the south, Morigaon district to the northeast, and Guwahati city to the west, it covers an area of 447.07 square kilometers. It comprises 12 gaon panchayats, 144 villages and a total population of 137,839 people [53]. The Brahmaputra River flows to the north of the block. Topographically, Dimoria exhibits a varied landscape of hills, plains, and isolated hillocks, representing an extension of the dissected Meghalaya plateau. Elevations range from 45 to 550 m above mean sea level, with the northern part characterized by alluvial plains and the southern part by hilly terrain. Lateritic soil is prevalent in the region. This topography significantly influences drainage patterns and contributes to flood vulnerability. The region's climate is subtropical monsoon, with an average annual rainfall of 1500 mm, primarily concentrated during the monsoon season. This intense rainfall, coupled with the undulating terrain and the presence of numerous streams and rivers, makes the area prone to flooding. Dimoria's forests are classified as semi-evergreen to mixed deciduous, with patches of subtropical broad-leafed forests. The area is rich in timber resources, including Sal, Gomari, Nahar, Poma, and Simalu. Land use is predominantly shifting cultivation practiced by tribal communities, alongside settled agriculture. The diverse land use patterns and forest cover play a role in influencing runoff and infiltration rates, further affecting flood dynamics.

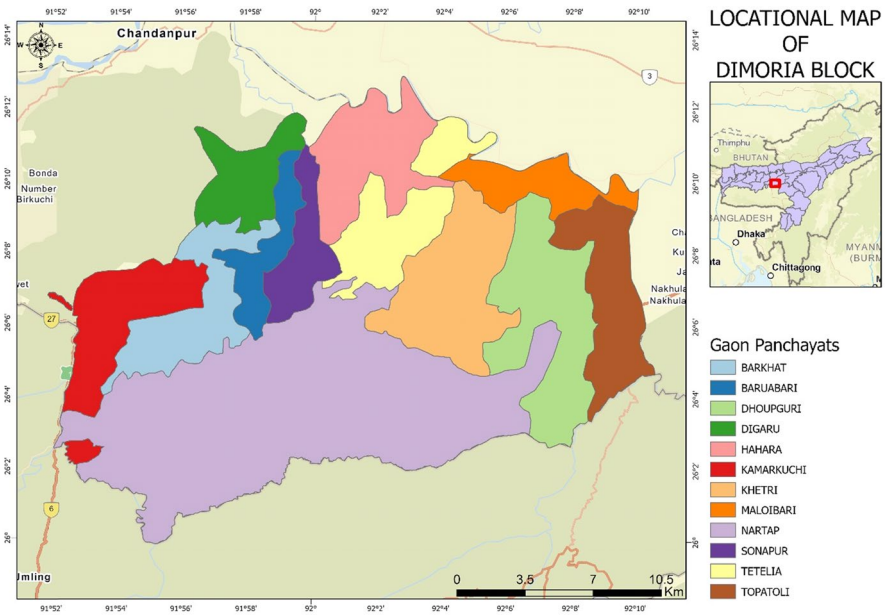

Fig. 1 Location map of the study area. This map shows the geographical extent and the administrative boundary of Dimoria Block within Kamrup Metropolitan District. The base map shows administrative boundaries, major roads, drainage network and neighboring units (Guwahati, Chandrapur Block, Morigaon District and Meghalaya) together with a north arrow and scale bar to aid orientation and interpretation

4 Database and methodology

4.1 Database

The present study involves both primary and secondary data integrated into a GIS interface. The detailed data descriptions have been provided in the table (Table 1). Flood susceptibility zones of the study area were determined using a multi-parametric dataset. Eleven influencing layers were considered: slope, elevation, rainfall, LULC, NDVI, soil, drainage density, distance from river, lithology, topographic roughness index (TRI), and sediment transport index (STI).

4.2 Methodology

The methodological flowchart of the present study can be seen in Fig. 2. The flowchart demonstrates the outline of the whole analysis, including generation of the flood influencing layers and developing the flood susceptibility map of the study area. The thematic database creation, basic statistical and sensitivity analyses have been performed by a composite utility of ArcGIS 10.3, ArcGIS Pro 2.8, EasyGPS and MS-Excel software. Multicollinearity analysis and Receiver Operating Characteristic-Area Under Curve (ROC-AUC) has been processed using IBM SPSS 20 software. Model validation includes the integration of the ROC-AUC, field verification and cross-validation with official reports.

GIS–AHP is often chosen for flood susceptibility mapping in data-scarce regions because it is transparent, easy to interpret, and does not require large historical datasets, unlike machine learning models which generally achieve higher accuracy but need substantial data for training and validation [54]. Fuzzy AHP can better handle uncertainty in expert judgment and may outperform classical AHP when expert opinions are inconsistent, but when the consistency ratio is acceptable, classical AHP is considered sufficient and simpler to implement [55].

The primary justification for selecting AHP in the present study is its simplicity and data efficiency, making it especially suitable for regions with limited or incomplete flood records, while still providing robust and reproducible results [54]. Although more complex methods like fuzzy AHP and machine learning can offer higher predictive

Table 1 Data descriptions

Data Type	Description	Source	Temporal Coverage/Year of Acquisition
Digital Elevation Model (DEM)	CartoDEM V3 R1 (30 m resolution)	Bhoonidhi https://bhoonidhi.nrsc.gov.in	2005–2014
Satellite imagery	ResourceSat 2-A LISS 4 (5.8 m resolution)	Bhoonidhi https://bhoonidhi.nrsc.gov.in	1 st November, 2023
Soil	Soil taxonomic map	NESAC https://nedrp.gov.in	2016
Lithology	Lithologic unit map	Bhukosh—Geological Survey of India https://bhukosh.gsi.gov.in	2018
Rainfall	The mean annual rainfall	CHRS Data Portal https://chrsdata.eng.uci.edu	1993–2023

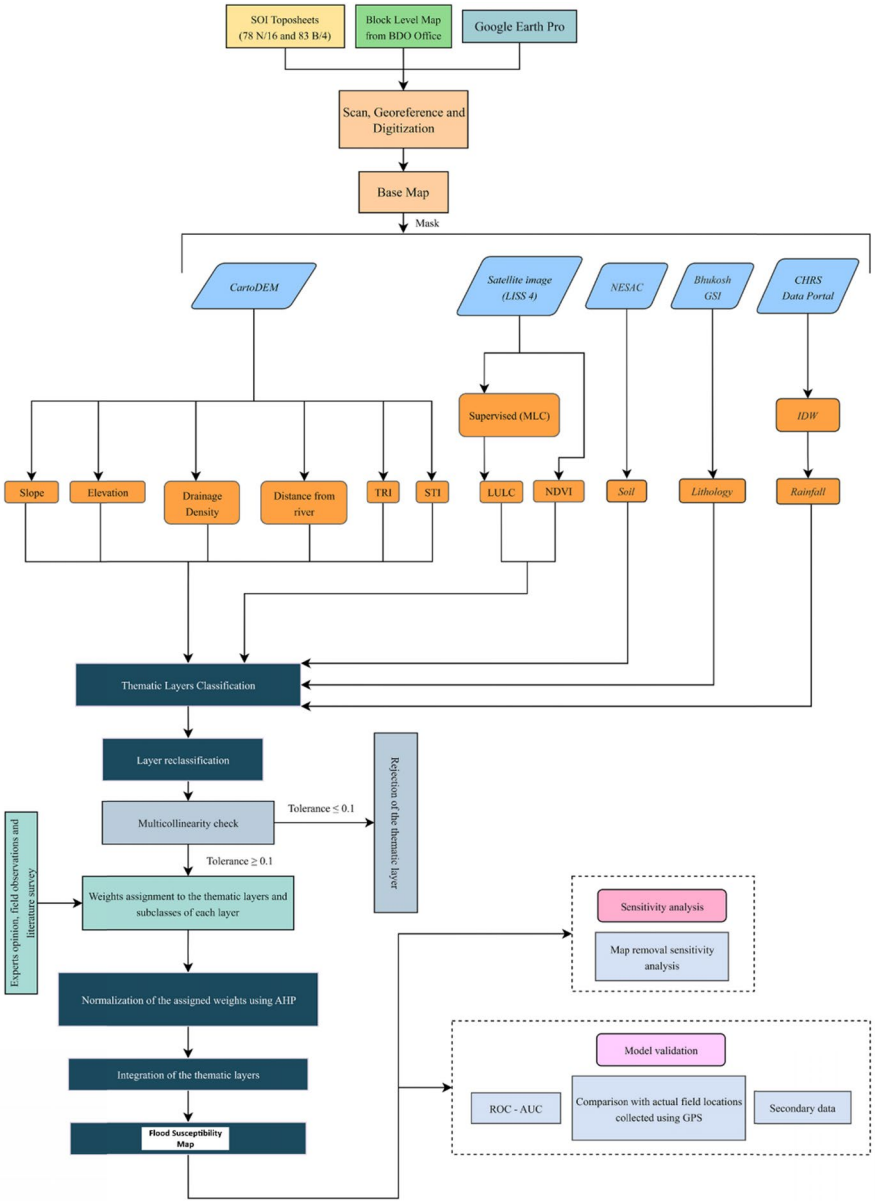

Fig. 2 Methodological flowchart for flood susceptibility mapping. This figure outlines the sequential process used to derive flood susceptibility zones, including data collection, thematic layer preparation, pairwise comparison and weighting using Analytical Hierarchy Process (AHP), raster standardization, GIS-based weighted overlay analysis, and final map generation. The flowchart provides a clear overview of how multiple data sources and criteria were integrated

accuracy, their added complexity and data requirements may not be justified when expert consistency is high and data are limited [55].

4.2.1 Preparation of flood influencing layers

The development of a flood susceptibility map of a given area is a complex process that requires the integration of multiple hydrological and terrain factors [44, 56]. Eleven flood-influencing parameters were selected for this study based on field observations

and a comprehensive literature survey [49, 57]. The selection of these parameters was guided by their well-established hydrological relevance, data availability, and documented roles in flood generation in comparable geomorphological settings. Previous GIS based flood susceptibility studies across India and other monsoon-dominated regions have consistently incorporated combinations of terrain factors (slope, elevation, TRI, TWI), hydrological variables (rainfall, drainage density, distance from stream), land cover indicators (LULC, NDVI), and surface characteristics (soil texture, lithology) to represent the multi-dimensional nature of flood behavior [58, 59]. Consultation of regional flood literature and expert judgement further supported the inclusion of these parameters, ensuring that both triggering forces (e.g., rainfall) and conditioning factors (e.g., geology, vegetation cover, terrain structure) were adequately represented. It is also recognized that AHP-based flood susceptibility modelling is sensitive to the number and selection of conditioning factors, since previous studies have applied varying numbers of parameters (e.g., seven to ten or more), depending on regional context and data availability [60, 61]. Thus, the final selection of eleven factors offers a comprehensive and robust framework for modelling flood susceptibility in Dimoria Block. A brief description of thematic layers generation has been outlined below:

CartoDEM V3 R1 (30 m resolution) data was downloaded from Bhoonidhi portal of ISRO to prepare the slope, elevation, drainage density, distance from river, TRI and STI maps, respectively. TRI is determined by the study basin's local topography and is calculated by [62]:

$$\mathrm{TRI} = \frac{(Area_V - Area_I)}{(Area_P - Area_I)} \tag{1}$$

where, $\mathrm{Area_V}$ ($\mathrm{A_V}$) = Variable Surface Area, $\mathrm{Area_P}$ ($\mathrm{A_P}$) = Planimetric Surface Area and $\mathrm{Area_I}$ ($\mathrm{A_I}$) = Area of interest.

STI can upturn the frequency of floods, resulting in foundation damage and is calculated by [63]:

$$\mathrm{STI} = \left(\frac{A_s}{22.13}\right)^{0.6}\left(\frac{Sin_\beta}{0.0896}\right)^{1.3} \tag{2}$$

where, '$\mathrm{A_s}$' = Upstream region and '$_\beta$' = Slope of each pixel.

Distance from river (km) was produced by overlaying the DEM of the study area and river shapefile extracted from the high-resolution satellite imagery. The Euclidean Distance tool of ArcMap was used to generate the thematic layer, following standard practices adopted in previous flood susceptibility studies [13, 43]. The drainage density map was also prepared using the downloaded DEM. With ArcMap's hydrology and density tools, the drainage density map was created.

ResourceSat-2A LISS 4 satellite imagery was downloaded from the Bhoonidhi portal of ISRO to prepare the LULC and NDVI maps having spatial resolution of 5.8 m, captured on November 1 st 2023. The LULC map has been prepared using maximum likelihood classifier (MLC), a supervised classification algorithm. The Normalized Difference Vegetation Index (NDVI) is a widely used remote sensing metric that

provides valuable insights into the health and vibrancy of vegetation. It is calculated as a normalized ratio between visible red (B3) and near infrared bands (B4) [64]:

$$NDVI = \frac{NIR(B4) - Red(B3)}{NIR(B4) + Red(B3)} \tag{3}$$

Soil map of the study area bearing a scale of 1:250,000 was prepared from the "NESAC Geo Portals". Lithology map was prepared from the data derived from GSI Bhukosh.

Precipitation data were obtained from the Center for Hydrometeorology and Remote Sensing (CHRS) for the period 1993–2023. The PERSIANN-CDR dataset, provided as a gridded raster product with a spatial resolution of 0.25° × 0.25°, was used in this study. Mean annual rainfall values corresponding to the study area were extracted from the PERSIANN-CDR raster at twelve representative locations, namely Marang Dala, Khat Tetelia N.C., Barkuchi N.C., Bajeni Gaon, Damara Pathar, Khaloibari Gaon, Murkata, Dakhin Dimoria, Tepechia Gaon, Juboi, Maloibari Gaon, and Sonapur Pathar. The number of extraction locations was selected to correspond with the twelve Gaon Panchayats within Dimoria Block, ensuring uniform spatial representation across the study area and alignment with local administrative units relevant for flood management and planning. To generate a spatially continuous rainfall surface compatible with other thematic layers used in the GIS–AHP framework, the extracted rainfall values were interpolated using the Inverse Distance Weighted (IDW) method. IDW assigns weights to surrounding values based on their distance from the prediction location, assuming that spatial influence decreases with increasing distance [63]. This interpolation step was applied for spatial harmonization and visualization purposes rather than to reconstruct rainfall measurements, as the source dataset is already provided in gridded raster format. The IDW formulation used for spatial interpolation is expressed as [65]:

$$\mathrm{Zp} = \frac{\sum_{i=1}^{n} \left(\frac{Z_i}{d_i^p} \right)}{\sum_{i=1}^{n} \left(\frac{1}{d_i^p} \right)} \tag{4}$$

where, Z_p = Predicted value, Z_i = value at i measured point, d_i = distance of i measured location to the predicted point, p = power function and n = number of points to be used. The power value 'p' determines how much known interpolated values counts based on the distance between the point and the output point. It is a positive, real number and the default value is always 2. A higher power value gives more weight to nearby points, increasing the impact of local data and creating a less smooth, more complex surface. A lower power value, however, extends influence further, resulting in a smoother output [63].

All the thematic layers thereupon were transformed to Projected Coordinate System (PCS) of UTM zone 46 N and resampled to a resolution of 5 m. The natural breaks (jenks) method was applied to group the values of the quantitative variables such as elevation, slope, drainage density etc. The Natural Breaks classification method is widely used in MCDA and machine learning because it effectively divides

data into distinct clusters based on inherent groupings [44], good adaptability, and high accuracy on the geographical environment [66, 67]. We used this method since it is capable in maximizing the variability between classes and lowering variability within a category. It makes sure there is the optimum distinction of various classes groups around the average and the minimization of variation of each class. It aids in formation of statistically homogeneous groups; hence it is an efficient method of grouping variables affecting flood hazard [44].

The number of classes assigned to each flood-conditioning factor was determined based on the data distribution using the Natural Breaks (Jenks) classification method, which minimizes variation within each class and maximizes the difference between classes [68, 69]. Factors with more widely dispersed data, e.g., slope, and elevation, were naturally found to have more statistically significant breakpoints and were thus grouped into five classes, whereas variables with more narrow ranges, or categorical constraints, e.g., NDVI, were found to have fewer significant divisions and were therefore grouped into three or four classes. These are the data-based class boundaries that are used to avoid arbitrary thresholding and enhance the sensitivity of the model by making sure that between classes, there is a geomorphic and hydrological variability. In addition, since weights of AHP are provided to class intervals instead of raw values, proper selection of classes improves the credibility and steadiness of the final susceptibility map by decreasing the level of classification prejudice [70].

4.2.2 Multicollinearity diagnosis

Multicollinearity diagnosis was performed to check the problem of strong linear relationship among the explanatory variables. It affects the prediction accuracy of the model [57, 71]. Hence, two indicators are used: Variance Inflation Factor (VIF) and Tolerance (TOL) [58]. If the threshold value of VIF is > 5 and TOL is < 0.1, then multicollinearity exists [71]. Table 2 shows the absence of multicollinearity problem among the variables used in this study. TOL and VIF are calculated by [71]:

Table 2 Multicollinearity analysis

Parameters	Tolerance (TOL)	Variance Inflation Factor (VIF)
Slope	0.488	2.049
Elevation	0.427	2.341
Rainfall	0.705	1.418
LULC	0.371	2.695
NDVI	0.395	2.531
Soil	0.631	1.584
Drainage Density	0.458	2.183
Distance from River	0.610	1.639
Lithology	0.793	1.261
TRI	0.406	2.463
STI	0.440	2.272

(Source: Calculated by the authors)

$$TOL = 1 - R_j{}^2 \tag{5}$$

$$\text{VIF} = \frac{1}{TOL} \tag{6}$$

where $R_j{}^2$ = coefficient of determination.

4.2.3 Analytical hierarchy process (AHP)

The reclassified layers were subjected to overlay analysis. The Weighted Overlay tool allows the incorporation of varied factors and their importance (weights) into decision-making models, crucial for environmental planning, cumulative impact assessment, and benefiting from integrated human judgment [65]. One of the best techniques for integration is the Analytical Hierarchy Process (AHP), which gives various weights to each flood-related element. It is a flexible and organized method for deciphering multi-factor difficult decision scenarios [72]. A flood hazard map was produced by superimposing the parameters according to weights that have been assigned. The assigned weights were determined based on expert judgement, literature review and field observation so as to indicate their relative significance within the context of the study. For instance, in our study LULC received more weight (11.1%) than context-specific variables such as soil (5.8%) and lithology (7.8%) since LULC have been identified as one of the most influential factors in various flood susceptibility studies [73, 74]. In many contexts, it contributed to overall flood susceptibility by more than 60 percent, over that of soil and lithology [75, 76]. Hence the weight assignment procedure is resonated. Even such context-specific weight assignment has also been adopted in studies by [58].

The generated weights were between 0–9, based on Saaty's fundamental scale. AHP served as a way to categorize various criteria within the criterion into various suitability levels [77]. Thomas L. Saaty based AHP on his experience and created it in 1977 [78]. He established the consistency ratio (CR), which is the ratio of the random index (RI) to the consistency index (CI), to assess the consistency of the matrix. If CR < 0.1, it can be considered suitable for additional examination. The matrix's characteristics determine the RI, which is a fixed number. The following formula ensures consistency [78]:

$$\text{CR} = \frac{CI}{RI} \tag{7}$$

$$\text{CI} = \frac{\lambda_{max} - n}{n - 1} \tag{8}$$

where, n is the number of components, λ_{max} is the matrix's Principal Eigenvalue, CI is the consistency index, RI is the random index, and CR stands for consistency ratio [72]. The primary Eigenvalue is obtained by multiplying each element of the Eigenvector by the total number of columns of the reciprocal matrix [77]. Table 3 shows Saaty's fundamental scale of relative importance [78], based on which the pairwise comparison matrix was generated. In this paper, the percentage of weight is generated using a pairwise comparison matrix table (Table 4) ranging the class 1–5 (very low to very high) based on the significance of each class of each flood causative criterion.

Table 3 Saaty's scale of relative importance

Intensity of importance	Definition
1	Equal importance
3	Moderately importance
5	Strongly importance
7	Very strongly importance
9	Extremely importance
2,4,6,8	Intermediate values

In order to reduce subjectivity and possible weighting biases of expert-based AHP pairwise comparisons, the judgments were cross-referenced and validated to make hydrological sense. The prioritization of the criteria was checked with the existing literature and field knowledge to prevent excessive or insufficient weighting of any of the parameters. Also, the Consistency Ratio (CR ≤ 0.10) was verified to ensure that the comparisons were within acceptable range hence limiting the inconsistencies and tonal bias in the assignment of weights.

4.2.4 Sensitivity analysis

Sensitivity analysis is an important step to understand the influence of each factor on the output model [79, 80]. It shows which layer(s) is/are the most/least critical in determining the values of the output map [81]. In our study, we adopted the map removal method [82]. In this method, one influencing layer is removed at a time and a new flood susceptibility map is created by overlaying the remaining layers [79, 83]. It is expressed as 'Sensitivity Index (SI)' calculated by [28]:

$$SI = \frac{\left|\left(\frac{FRZ}{N}\right) - \left(\frac{FRZ'}{n}\right)\right|}{FRZ} * 100 \tag{9}$$

where FRZ = Flood Risk Zonation of all layers, FRZ′ = Flood Risk Zonation of one excluded thematic layer, N = number of thematic layers in FRZ and n = number of thematic layers in FRZ′.

4.3 Model validation

Model validation is a crucial part to understand the model's effectiveness and applicability [84, 85]. The ROC-AUC curve is a widely used method of validation particularly in flood hazard studies due to its reasonable, logical, and easily understandable method [84]. On the two-dimensional ROC graph, the y-axis stands for sensitivity (true positive rate) and the x-axis represents 1-specificity (false positive rate) [58]. It is given by [86]:

$$x = 1 - Specificity = 1 - \left[\frac{TN}{TN + FP}\right] \tag{10}$$

Table 4 Pairwise comparison matrix

Parameters	Slope	Elevation	Rainfall	LULC	NDVI	Soil	Drainage Density	Distance from River	Lithology	TRI	STI
Slope	1	1	1/3	1/2	1/2	1/3	1/2	1/3	1/3	1/2	1/3
Elevation	1	1	1/3	1/2	1/2	1/3	1/2	1/3	1/3	1/2	1/3
Rainfall	3	3	1	2	2	3	2	3	3	2	5
LULC	2	2	1/2	1	1	2	1	2	2	1	3
NDVI	2	2	1/2	1	1	2	1	2	2	1	3
Soil	3	3	1/3	1/2	1/2	1	1/2	1/3	1/3	1/2	1/3
Drainage Density	2	2	1/2	1	1	2	1	2	2	1	3
Distance from River	3	3	1/3	1/2	1/2	3	1/2	1	1	1/2	1
Lithology	3	3	1/3	1/2	1/2	3	1/2	1	1	1/2	1
TRI	2	2	1/2	1	1	2	1	2	2	1	3
STI	3	3	1/5	1/3	1/3	3	1/3	1	1	1/3	1

(Source: Calculated by the authors)

$$y = Sensitivity = \left[\frac{TN}{TP - FN}\right] \tag{11}$$

where TP = True Positive, TN = True Negative, FP = False Positive and FN = False Negative.

5 Results

5.1 Flood hazard indicators

5.1.1 Slope

One of the hydrology keys that should be considered in understanding flood event dynamics is slope. Aggregating slope angles can symbolize an area's susceptibility to flooding [84]. The present result states that 41.35 percent of the land has a slope 0- 5.4°. This is typically a gentle slope because its original ability to properly drain water has been lost [87]. At the same time, less than 2.8 percent of the land is slopes steeper than 54.8°, while the area occupied by elevations of 26.5–54.8° is just 7.65 percent (Fig. 3). In fact, these steeper slopes let the faster water flow and a lower likelihood of flooding later [88]. The hydrological behavior of the area is very sensitive to slope angle in the area [63]. The slope angle gives us important information about the likelihood of such occurrences, and therefore flood control techniques are directed at the overflow.

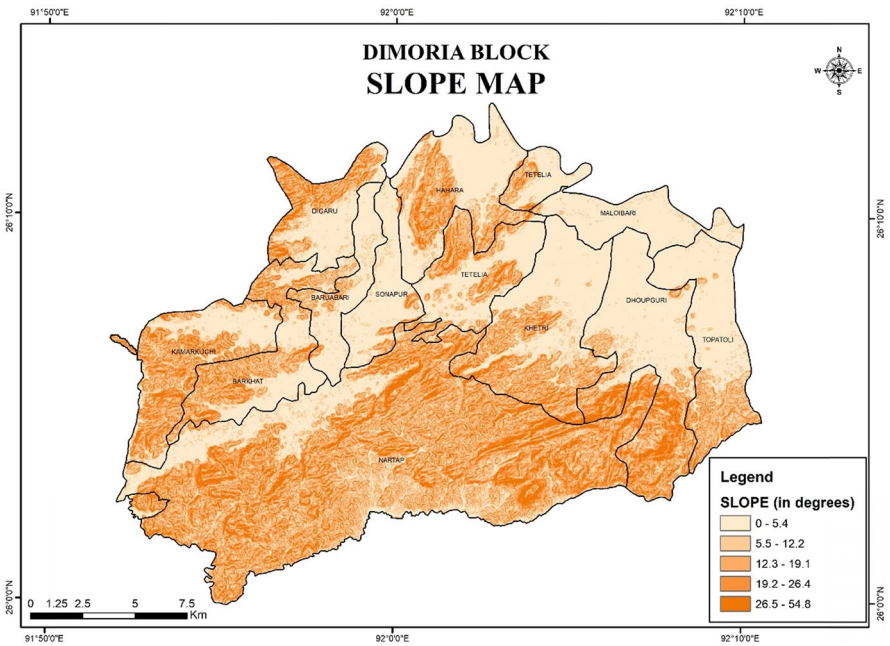

Fig. 3 Slope map of Dimoria Block. The map shows spatial variations in terrain slope expressed in degrees, categorized into five classes ranging from nearly flat (0°–5.4°) to steep (26.5°–54.8°). The map uses a rusty brown color gradient to represent slope, ranging from very lighter shade to darker shade. Lower slope areas, primarily in central and northern Dimoria, represent relatively flat surfaces susceptible to water stagnation and flooding, while steeper slopes occur along the southern uplands near Meghalaya and western Dimoria. Administrative boundaries, a north arrow, and a scale bar support interpretation

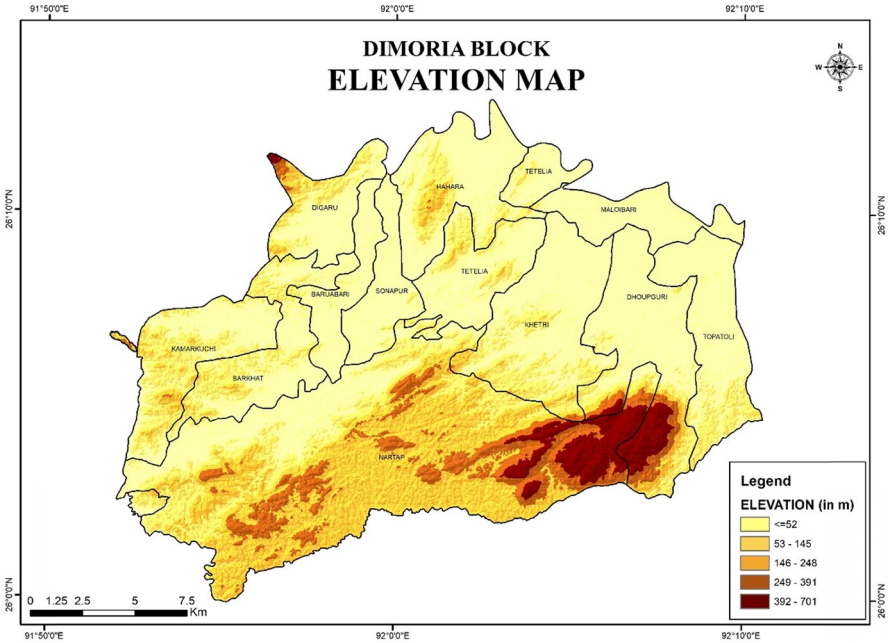

Fig. 4 Elevation map of Dimoria Block. The map presents elevation classes indicating the vertical relief of the landscape. The map uses a brown color gradient to represent elevation, ranging from very light brown (low-lying areas) to dark brown (higher terrain). Low-lying alluvial plains in central and northern parts (≤ 52 m) correspond to higher flood susceptibility, whereas elevated zones in the south exhibit reduced flood likelihood. The map includes administrative limits, a north arrow, and a scale bar for clarity

5.1.2 Elevation

A fundamental characteristic in geographic terms, the elevation of a given area is a key to understand and predict flood susceptibility in that region. The results show that the area of less than 52 m makes a larger per cent of the total area followed by the areas that have an elevation of 53–145, 146–248 m, 249–391 m and 392–701 m respectively (Fig. 4). The finding suggests in terms of flooding, the areas below 52 m high are the most vulnerable [45, 89]. The water more often flows and accumulates in these low-lying areas during high water level periods [90]. In addition, residential areas and farming fields often exist in these flood prone, low-lying areas making them vulnerable to the social and economic impacts of floods; loss of life and property damage [89]. Whereas, the areas at the higher elevations are less susceptible for flooding because the topography of these places is unlikely to trap water [45, 91].

5.1.3 Rainfall

Rainfall is a primary determinant of flooding in a region [63], and flood events may result from intense precipitation occurring over short time periods. Rainfall therefore plays a key role in the occurrence of floods in Dimoria Block. Excessive monsoon rainfall contributes to increased discharge in the Kalang and Digaru rivers, leading to overbank flow and inundation of adjacent floodplains. Rainfall data covering a period of more than 30 years (1993–2023) were obtained from the PERSIANN-CDR dataset. Mean annual rainfall values extracted at representative locations within the study area were used to generate a continuous rainfall surface. The rainfall distribution was classified into five

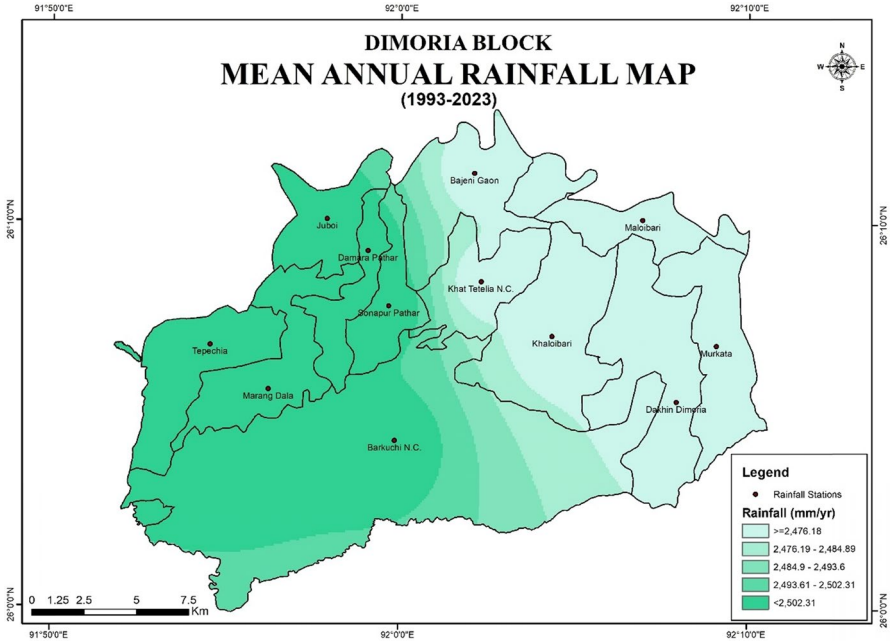

Fig. 5 Rainfall distribution map of Dimoria Block. The map illustrates the spatial variation in mean annual rainfall derived from the PERSIANN-CDR dataset (CHRS), with values extracted at twelve representative locations corresponding to the twelve Gaon Panchayats and interpolated to generate a continuous surface. Rainfall values are classified into five categories. A light-to-dark blue color gradient represents increasing rainfall magnitude, with lighter shades indicating lower rainfall and darker shades indicating higher rainfall. The map also includes administrative boundaries, a north arrow, and a scale bar for spatial reference

categories ranging from very low to very high rainfall (Fig. 5). The mean annual rainfall exhibits a gradual increase from east to west across the study area.

5.1.4 Land use and land cover (LULC)

The landuse and land cover constitute waterbodies (1.05%), vegetation (49.02%), built up (4.80%), and agricultural (45.13%) in the study area (Fig. 6). The flood susceptibility of the region is directly linked to the LULC pattern [58]. Although a relatively small portion of the area is waterbodies, they can act as natural flood buffers. As only 1.05 per cent of the region comprises waterbodies, it has limited natural flood storage capacity. Waterbodies such as lakes, wetlands, and floodplains can provide important attenuating flood flow and reduce downstream flood susceptibility. Additionally, high percentage of vegetation cover (49.02%) implies the landscape has a remarkable capacity to store and slow water flow through its flood events [92, 93]. Rainfall interception, increase soil infiltration and reduce surface runoff by vegetation (especially dense and deep rooted) reduces the susceptibility to flooding [93]. However, more of the landscape is built-up area or agricultural land that represents nearly 50% of the total. Urban development and agricultural practices which create impervious surfaces associated with disrupted drainage patterns favor increased surface runoff and enhanced flood hazards [93, 94].

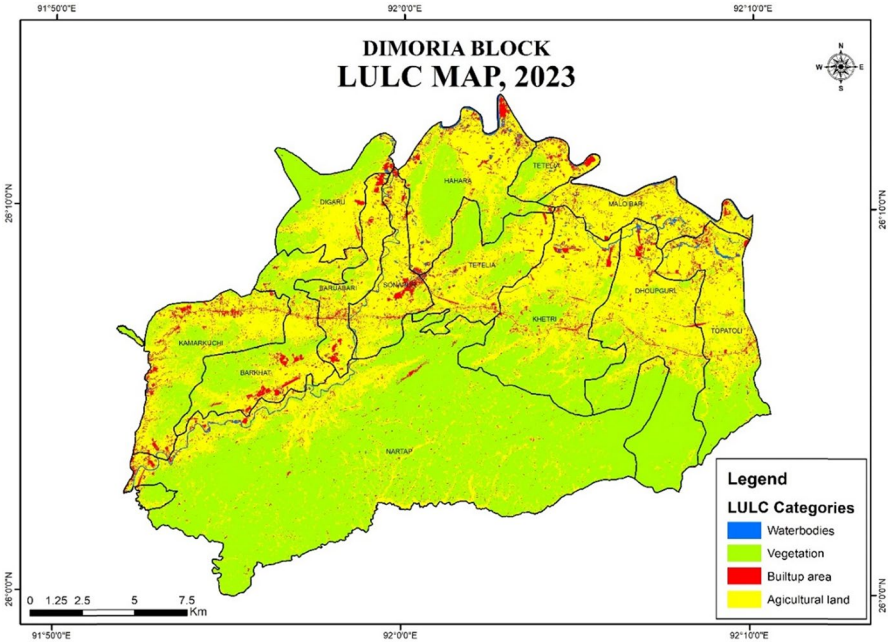

Fig. 6 LULC map of Dimoria Block. The map classifies the block into four major LULC categories such as waterbodies, vegetation, built-up areas and agricultural land. Each class is colour-coded to indicate land characteristics influencing runoff and infiltration. Agricultural and built-up zones correspond to higher flood susceptibility, primarily situated in the low-lying alluvial plains while vegetated areas indicate lower vulnerability, primarily found in the southern parts and uplands of the region. Administrative boundaries, drainage patterns, north arrow, and scale bar are provided

5.1.5 Normalized difference vegetation index (NDVI)

NDVI is mainly utilized to monitor the vegetation. However, in recent studies, efforts are made to understand the dynamics of the flood events using this parameter [28]. Vegetation is significantly affected by floods and may result in decreased photosynthetic activity and altered spectral reflectance of affected areas [95]. It allows researchers to understand how severe and deep the flood impact was on the local vegetation by analyzing their NDVI patterns. The use of NDVI values in the present analysis adds to the understanding of the possible correlation between vegetation and flood occurrences. Provided that a significant proportion (59.48%) of the study area is characterized by high NDVI values (suggestive of a relatively healthy and resilient vegetation cover that is capable of at least partially mitigating flood impacts [64], the potential presence of land management practices alleviating the impact of flood events can be considered. On the other hand, the areas featuring the lower NDVI values and a lesser portion of an area can signal distressed or degraded vegetation (which could be the indication of the damages caused by recent flood events). This could occur among the moderate NDVI values, which may represent areas that have been partially flooded or areas recovering. NDVI patterns can be interpreted as a basis for understanding the response of the vegetation to flood disturbances and potential role in reducing the impacts of floods (Fig. 7).

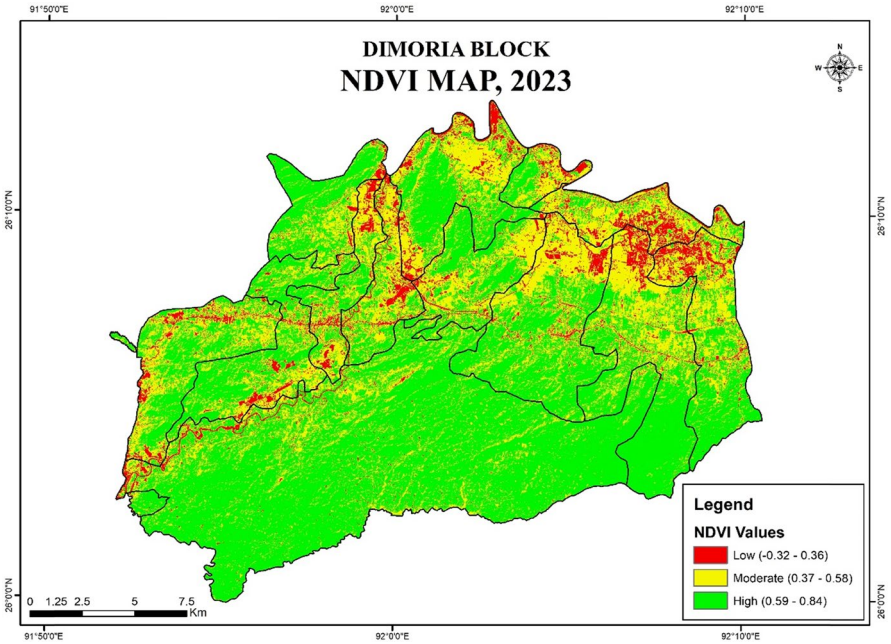

Fig. 7 NDVI map of Dimoria Block. The map shows vegetation health and density, classified into low (red), moderate (yellow), and high (green) NDVI values. Low NDVI regions correspond to sparse vegetation and higher surface runoff, typical of built-up areas and waterbodies. Whereas high NDVI areas indicate dense vegetation and reduced flood hazard, typical of vegetated areas of the region. The map includes administrative boundaries, drainage network, north arrow, and scale bar

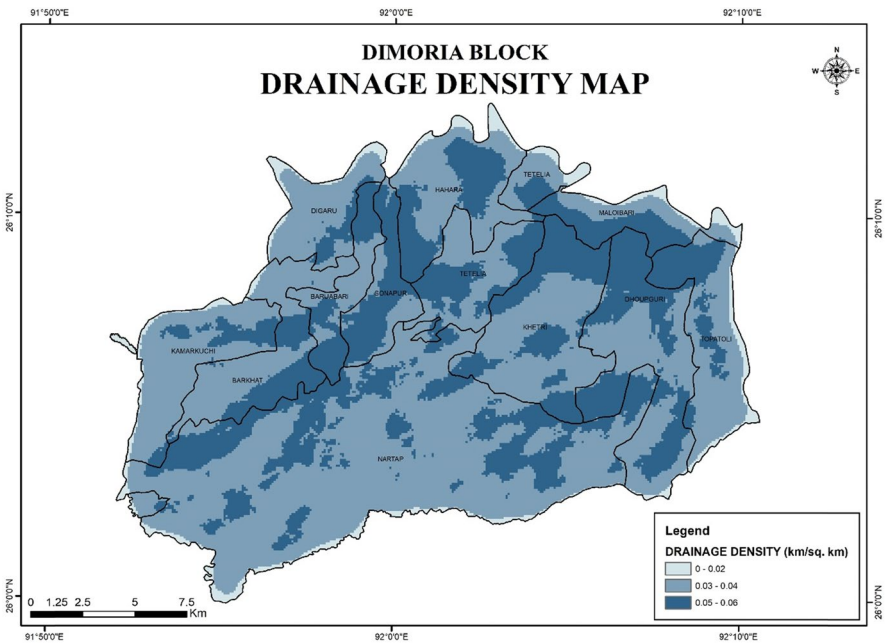

Fig. 8 Drainage density map of Dimoria Block. This map illustrates the density of stream channels per square kilometre, color-coded in shades of blue. Higher drainage density areas (0.05–0.06 km/sq. km) are depicted in dark blue and typically show higher runoff and increased flood potential. These are present in the low-lying areas of the region. Lower density zones (0–0.02 km/sq. km) are depicted in light blue and exhibit reduced susceptibility, are present in the uplands of the region. The map is supported by administrative boundaries, north arrow, and scale bar

5.1.6 Drainage density

Drainage density, a very important parameter in hydrology, is the sum of the total length of all streams and rivers present in each watershed recalled over the total area of the watershed [63]. The drainage density distribution within a region can offer important information about the possibility of flood happening. The study has presented the data which shows an interesting distribution of drainage density in interest, 9.45% of the land is drained from 0 to 0.02 km/sq km, 57.54 is from 0.03 to 0.04 km/sq km, and 33.01 is from 0.05 to 0.06 km/sq km respectively (Fig. 8). This distribution therefore suggests that there are a large proportion of the area that has a relatively moderate drainage density (57.54%), suggesting a greater susceptibility to flood events [96]. The infiltration capacity of the soil is inversely related to drainage density, and areas with high drainage density have lower infiltration rates which results in increased surface runoff and increased susceptibility to flooding [97].

5.1.7 Distance from river

Distance from river is a critical factor that can greatly influence both the occurrence and severity of floods [27]. River flooding occurs when a river overflows its banks, and a location's proximity to the river often determines how susceptible it is to inundation. It has been found that distance from the river, altitude, slope, and rainfall are among the most influential variables governing flood susceptibility in many regions [98]. As floods occur almost every year due to the Digaru and Kolong rivers [37], distance toward these two major rivers was measured and categorized into five classes, with Fig. 9 illustrating the decreasing flood susceptibility with increasing distance from the river.

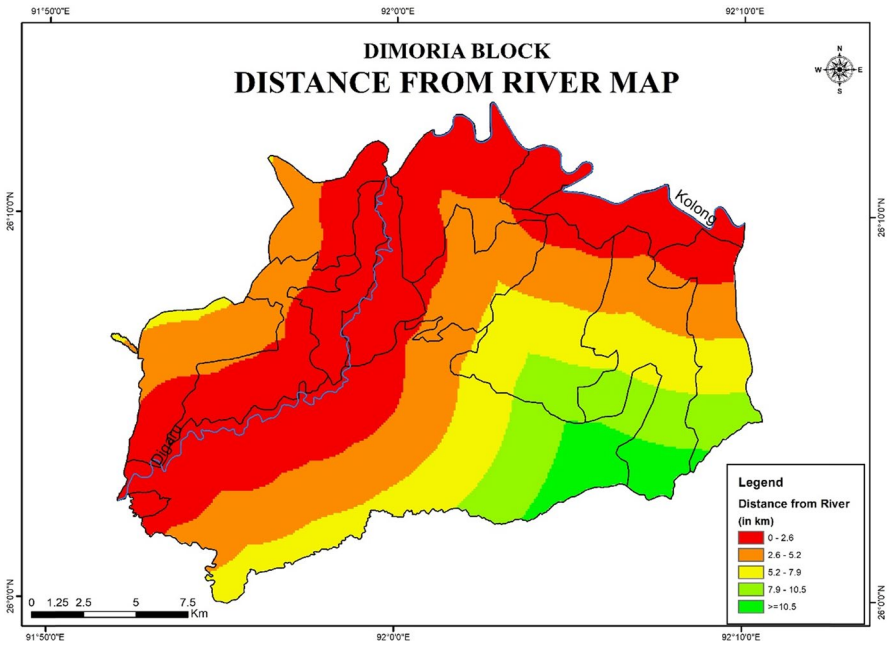

Fig. 9 Distance from river map of Dimoria Block. The map classifies land areas based on their proximity to major rivers such as Digaru and Kolong, expressed in km. Areas closest to river channels (red) exhibit the highest flood susceptibility, decreasing progressively with increasing distance (green). Administrative boundaries, drainage elements, north arrow, and scale bar aid interpretation

In the context of Dimoria Block, the distance from river analysis was intentionally limited to the Digaru and Kolong rivers because they constitute the primary hydrological systems responsible for monsoon-induced flooding [37]. Excluding minor streams and ephemeral channels is a common and justified practice in regional-scale flood susceptibility modeling as seen in [99–101]. Their influence is generally limited compared to major watercourses and other dominant factors. Hence, minor streams and ephemeral channels were also not included in the present study.

5.1.8 Topographic roughness index (TRI)

Vulnerability of a landscape to flooding events is related to topographic roughness index, an important parameter. It measures variability of the terrain, with larger values representing heavily rugged and heterogeneous terrain [62, 102]. The study area shows that the range of the topographic roughness falls within 0.11 to 0.41 (24.74%), 0.42 to 0.57 (54.11%), and 0.58 to 0.89 (21.15%) (Fig. 10). The results indicate that the region, which is 54.11 percent, has moderate topographic roughness, and that this is important for the susceptibility of floods. Such areas, with lower topographic roughness index values (0.11–0.41), are usually associated with less rugged or flat types of terrain that can promote rapid accumulation and movement of floodwaters [103]. On the other hand, areas with higher index values exhibit more diverse and undulating topography that can reduce the speed of moving flood waters and reduce the overall extent and impact of flood events [98].

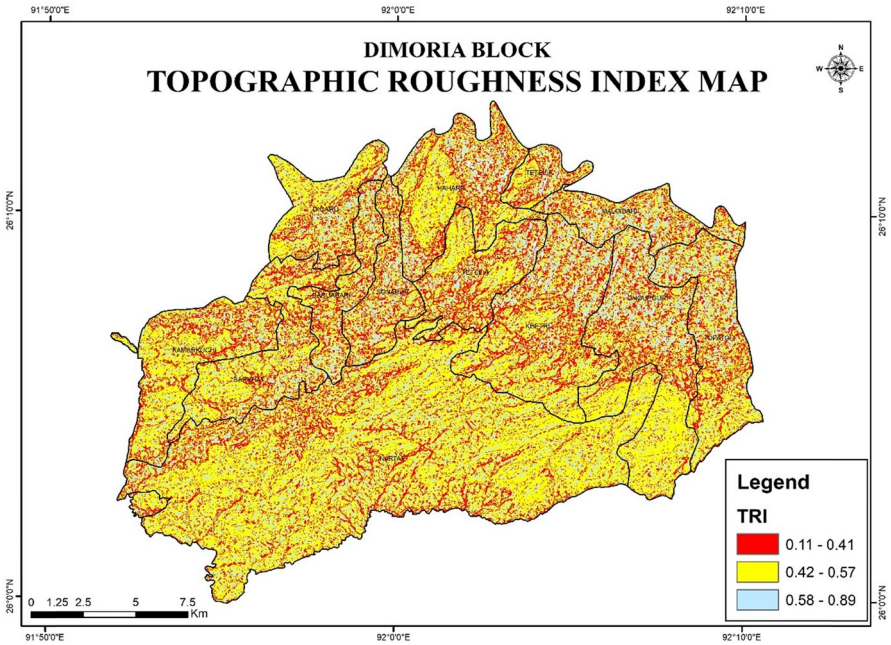

Fig. 10 TRI map of Dimoria Block. This map displays terrain irregularity, where low TRI values (red) represent smoother surfaces prone to inundation, while higher TRI values (light blue) correspond to rugged terrain with reduced flooding potential. Low TRI values are found in the low-lying alluvial plains of the study area whereas, high TRI values are found in the uplands of the study area. Administrative boundaries, drainage elements, north arrow, and scale bar aid interpretation

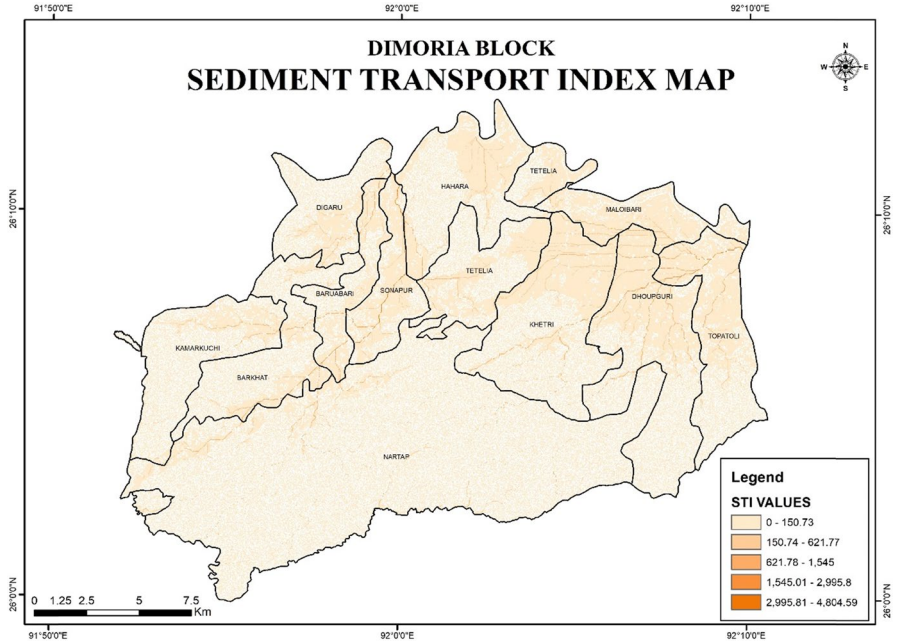

Fig. 11 STI map of Dimoria Block. The map shows the potential for sediment movement across the terrain and is classified into five classes. High STI regions (dark orange color) are found in the low-lying plains indicating greater sediment transport capacity, often associated with channel instability and increased flood susceptibility. Low STI regions (light orange color) are found in the uplands and indicate reduced flood susceptibility. The map provides administrative boundaries, drainage lines, north arrow, and scale bar to support interpretation

5.1.9 Sediment transport index (STI)

The amount of sediment transported by a river stream is quantified by the sediment transport index which can give us a clue on the likelihood of flooding. The observed wide range of sediment transport index values is quite large, from 0 to 150.73 to 2995.81 to 4804.59 (Fig. 11). As there is a very wide range in sediment transport index values, it is likely that the amount of sediment being transported can vary considerably with factors such as precipitation, slope, and channel geometry [63]. Heavy rainfall can trigger extreme flood events that generate a tremendous increase in sediment transport as landslides and surface erosion provide vast amounts of sediment to the river system [104]. This influx of sediment can lead to the channel becoming obstructed, which reduces its capacity to convey water and increases flood hazard [63].

5.1.10 Lithology

The study of lithology, the physical and mineralogical characteristics of rocks and sediments, bears critical importance to understanding responses of landscape to different environmental factors, during the time of floods. The analysis reveals that the lithological composition in this area is a considerable factor. In order of (proportion) the gneiss and migmatite/banded gneiss (unclassified gneiss and migmatite/banded gneiss) constitutes the largest part (60.96%), followed by unoxidised sand, silt, clay (28.12%), highly oxidized dark brown to red brown loamy sand (9.10%), grey to pink porphyritic granite (1.79%) and quartzite with thin phyllite interbands (0.05%).

With unclassified gneiss and migmatite/banded gneiss dominating the gneiss, the area appears to be underlain with metamorphic rocks, which are traditionally less permeable and less able to infiltrate [105]. Increased surface runoff and a greater likelihood of flooding during heavy rainfall events can arise from this. 24.7 per cent of the area is occupied by unconsolidated sediments which indicate that they are available to be developed for this purpose. These sediments are generally more prone to erosion and easy to be moved by the floodwaters, thereby disturbing sediment deposition in low lying locations and blockage of drainage systems [105]. Presence of highly oxidized dark brown to red brown loamy sand is likely to have resulted from well drained and weathered soils. They may have higher infiltration rate and lower water holding capacity leading to increased surface runoff and higher susceptibility of rapid flood events [106]. The small amount of grey to pink porphyritic granite and quartzite interbedded with thin phyllite may have igneous and metamorphic rocks that may act differently than their dominant lithologies (Fig. 12).

5.1.11 Soil

The susceptibility to flooding of an area can be explained in terms of soil composition and distribution. The results presented here suggest that the soil type to be found to be in the region is diverse and that influences on flood susceptibility are of varying degree. Fine, Typic Kandihumults-Loamy skeletal (Umbric Dystrochrepts), which makes up

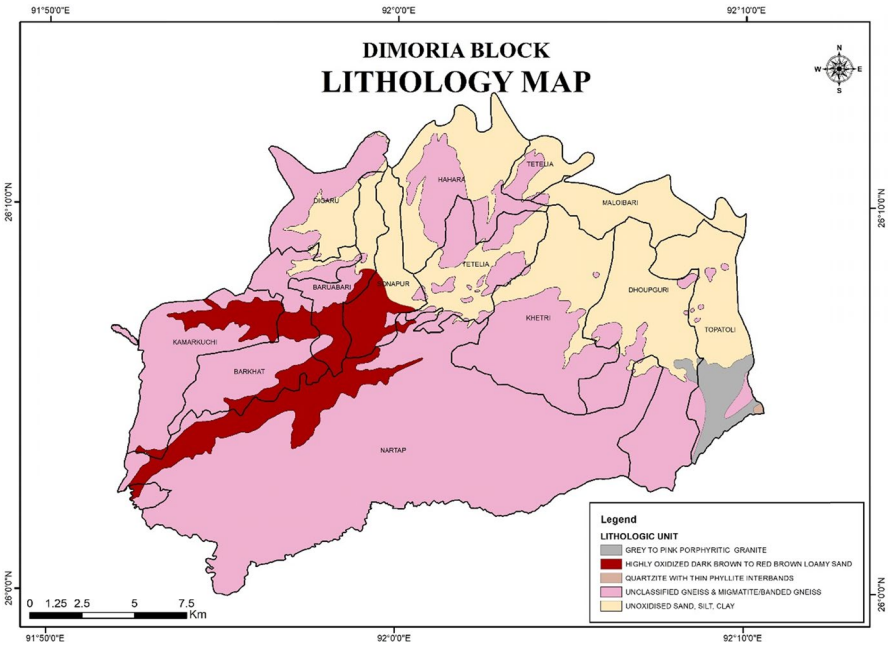

Fig. 12 Lithology map of Dimoria Block. This map depicts the distribution of major lithological units into five groups and coded with varying colors. The dominating lithological unit is unclassified gneiss and migmatite/banded gneiss which covers the southern, western, north-western and north-central portions of the region. On the other hand, grey to pink porphyritic granite and quartzite interbedded with thin phyllite are highly localized and are found in small proportions. These units influence infiltration rates and runoff behavior. The map includes administrative boundaries, north arrow, and scale bar for spatial reference

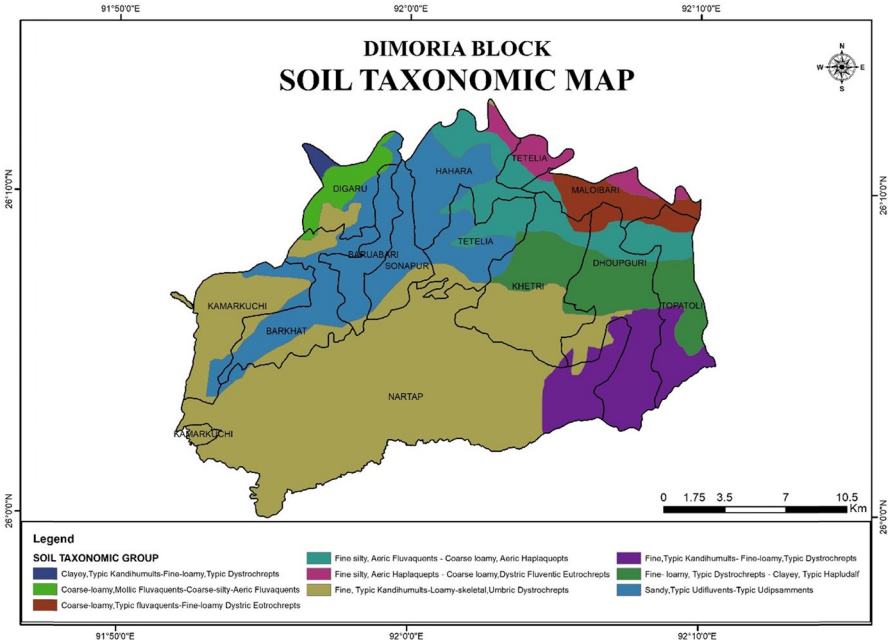

Fig. 13 Soil taxonomic map of Dimoria Block. The map categorizes soil types into nine groups, each color-coded to show the spatial variations. These soil groups influence water infiltration and flood behavior. Sandy loam areas exhibit higher infiltration and lower flood susceptibility, while clay-rich soils tend to retain water and increase flood likelihood. Administrative boundaries, drainage features, north arrow, and scale bar are provided

Table 5 Statistics of map removal sensitivity analysis

Parameter	Variation Index (%)			
	Minimum	Maximum	Mean	Standard Deviation
Slope	1.45	3.10	2.30	0.52
Elevation	1.20	3.00	2.10	0.58
Rainfall	8.80	19.20	14.40	2.65
LULC	5.10	14.12	9.61	1.92
NDVI	4.70	12.20	8.90	1.76
Soil	2.10	4.90	3.30	0.74
Drainage Density	4.94	12.74	8.60	1.88
Distance from River	3.26	7.21	5.07	0.93
Lithology	2.82	6.16	4.39	0.88
TRI	4.13	10.88	7.75	1.69
STI	2.91	7.07	4.96	0.96

(Source: Calculated by the authors)

47.08% of the area, is the predominant soil type. Typically, this soil type is fine textured and loamy-skeletal with moderate to high drainage capacity [106]. But in the affected areas, Umbric Dystrochrepts (a poorly drained soils type) also help increase the flood susceptibility [98]. Further details of the soil characteristics include Fine-loamy, Typic Dystrochrepts-Fine-loamy, Typic Dystrochrepts (8.92% of area) and Fine-loamy, Typic Dystrochrepts-Clayey, Typic Hapludalf (8.46% of area). These soils of fine-loamy and

clayey textures can be hampered to water infiltration, resulting in soil surface runoff and heightened possibility of flooding [106]. The deposition of Aeric Haplacept and Fluvaquent which is linked with wetlands and floodplains indicate that these lands are naturally more prone to flooding [89]. Soils of these soil types often have the coarse loamy and fine silty textures that further contribute to their limited drainage capacity and are likely to be more prone to waterlogging and inundation [107] (Fig. 13).

5.2 Sensitivity analysis

The map removal sensitivity analysis (Table 5) indicates rainfall (14.40%) and LULC (9.61%) had the greatest variation index with a high impact on the final flood susceptibility map. Contrastingly, elevation (2.10%) and slope (2.30%) had relatively low variation index having no significant influence when omitted. This variation indicates that rainfall and LULC are the most sensitive parameters of the model. It confirms the hydro-geomorphic circumstances of the region, which is primarily characterized by seasonal monsoons and the effect of land use changes on flood dynamics. Rainfall and LULC are always ranked as the greatest contributors to flood hazard in terms of integrated GIS-AHP as seen in studies by [48, 85].

Rainfall is the main driving force of surface runoff and LULC is the determinant of the infiltration capacity, evapotranspiration and surface roughness. These factors, in turn, influence how precipitation is converted into overland flow [108, 109]. By comparison, conditioning terrain factors include NDVI, drainage density, and TRI; these factors control the spatial distribution of conditions but have no direct causative role in causing flooding [108, 109]. NDVI represents vegetation cover, which mitigates runoff through interception and soil protection, although its influence varies with rainfall intensity [95]. Drainage density and TRI capture key geomorphological controls that regulate the speed and efficiency of surface water movement [108]. Their high weights highlight their importance in shaping flood response, but they function in conjunction with the dominant rainfall–LULC interaction. Thus, although several parameters show comparable weights, rainfall and LULC remain the primary causal factors governing flood susceptibility. The higher-weighted geomorphic variables (NDVI, drainage density, and TRI) mainly explain the spatial variation in flood intensity rather than the occurrence of flooding itself [108, 109]. The mean variation index across the layers reflects a consistent and balanced contribution of each factor in the AHP model, reinforcing the reliability and stability of the assigned weights.

6 Discussion

The flood susceptibility map was generated by overlaying eleven influencing layers using a combination of the AHP approach and the weighted overlay method (Fig. 14). The final map integrates eleven parameters with assigned weights of slope (4.1%), elevation (4.1%), rainfall (19.3%), LULC (11.1%), NDVI (11.1%), drainage density (11.1%), distance from river (7.8%), TRI (11.1%), STI (5.7%), lithology (7.8%), and soil (6.8%), respectively (Table 6). Although LULC, NDVI, drainage density, and TRI exhibit similar AHP-derived weights, their functional roles differ: LULC directly influences runoff generation

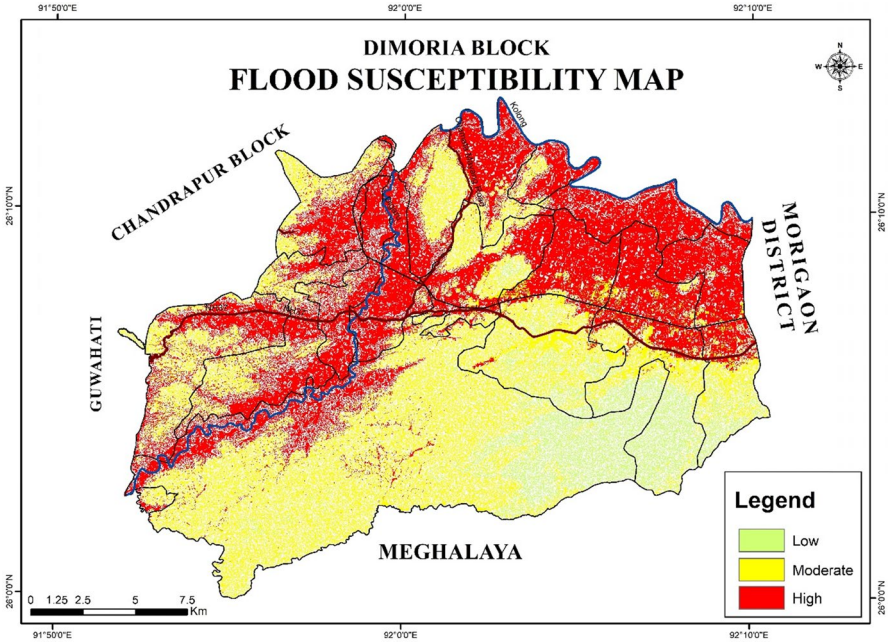

Fig. 14 Flood susceptibility map of Dimoria Block. This map illustrates the spatial distribution of flood susceptibility zones generated through GIS-based weighted overlay analysis using AHP-derived weights. The block is classified into three categories: low susceptibility (light green), moderate susceptibility (yellow), and high susceptibility (red). High susceptibility areas are concentrated along major river channels and low-lying alluvial zones in central and northern Dimoria. Moderate susceptibility zones form transitional bands, while low susceptibility areas lie mainly in the elevated southern section bordering Meghalaya. The map includes administrative boundaries, major roads, drainage lines, neighboring regions, a north arrow, and scale bar

processes, whereas NDVI, drainage density, and TRI primarily act as conditioning factors controlling the spatial distribution and magnitude of flooding [108, 109].

The study follows the weight assignment approach proposed by [78], where higher values indicate greater relative importance and lower values indicate lesser influence. Rainfall received a higher weight than other variables, reflecting its dominant role in flood generation within the study area. The region largely functions as a rainfed system, and flood occurrence is directly influenced by rainfall variability. Intense rainfall and flood events frequently occur in the study area, which lies within the Brahmaputra valley region [53]. Elevation and slope were assigned lower weights due to the relatively uniform topographic characteristics of the terrain. The analysis satisfies the methodological criteria of [78], as the calculated consistency ratio (CR) remains below the acceptable threshold of 0.1, with a value of 0.0610 (6.1%).

The evaluation process classified the study area into three flood susceptibility categories: low, moderate, and high. Low susceptibility zones account for 8.52% (38.11 km^2) of the total area, while high susceptibility zones comprise 54.75% (244.74 km^2). Moderate susceptibility zones occupy 164.22 km^2 (36.72%) of the study area (Table 7).

High susceptibility zones are primarily concentrated in low-lying floodplains characterized by gentle slopes, proximity to river channels, and higher rainfall accumulation. The lithological composition in these areas is predominantly unconsolidated, consisting of loose sedimentary materials and poorly drained soils, which contribute to increased flood susceptibility. The shallow and meandering

Table 6 Sub criteria of each parameter and their weights

Flood Causative Criterion	Unit	Class	Ranking (Very high = 5, Very low = 1)	Weight (%)
Slope	°	0–5.4	5	4.1
		5.5–12.2	4	
		12.3–19.1	3	
		19.2–26.4	2	
		26.5–54.8	1	
Elevation	m	< = 52	5	4.1
		53–145	4	
		146–248	3	
		249–391	2	
		392–701	1	
Rainfall	mm/year	> = 2476.18	1	19.3
		2476.19–2484.89	2	
		2484.90–2493.60	3	
		2493.61–2502.31	4	
		< 2502.31	5	
LULC	Class	Waterbodies	5	11.1
		Vegetation	1	
		Builtup area	4	
		Agicultural land	3	
NDVI	Values	−0.32–0.36	5	11.1
		0.37–0.58	4	
		0.59–0.84	3	
Soil	Class	Fine, Typic Kandihumults-Loamy-skeletal,Umbric Dystrochrepts	1	6.8
		Fine,Typic Kandihumults- Fine-loamy,Typic Dystrochrepts	2	
		Fine- loamy, Typic Dystrochrepts—Clayey, Typic Hapludalf	3	
		Fine silty, Aeric Haplaquepts—Coarse loamy,Dystric Fluventic Eutrochrepts	2	
		Coarse-loamy,Typic fluvaquents-Fine-loamy Dystric Eotrochrepts	4	
		Fine silty, Aeric Fluvaquents—Coarse loamy, Aeric Haplaquepts	5	
		Coarse-loamy,Mollic Fluvaquents-Coarse-silty-Aeric Fluvaquents	3	
		Sandy,Typic Udifluvents-Typic Udipsamments	1	
		Clayey,Typic Kandihumults-Fine-loamy,Typic Dystrochrepts	4	
Drainage Density	km/sq. km	0–0.02	3	11.1
		0.03–0.04	4	
		0.05–0.06	5	
Distance from River	km	0–2.6	5	7.8
		2.6–5.2	4	
		5.2–7.9	3	
		7.9–10.5	2	
		> = 10.5	1	

Table 6 (continued)

Flood Causative Criterion	Unit	Class	Ranking (Very high = 5, Very low = 1)	Weight (%)
Lithology	Class	Unoxidised Sand, Silt, Clay	5	7.8
		Highly Oxidized Dark Brown to Red Brown Loamy Sand	4	
		Unclassified Gneiss & Migmatite/ Banded Gneiss	2	
		Grey to Pink Porphyritic Granite	1	
		Quartzite with Thin Phyllite Interbands	3	
TRI	Level	0.11–0.41	5	11.1
		0.42–0.57	4	
		0.58–0.89	3	
STI	Level	0–150.73	5	5.7
		150.74–621.77	4	
		621.78–1545.00	3	
		1545.01–2995.80	2	
		2995.81–4804.59	1	

(Source: Calculated by the authors)

Table 7 Categorization of Flood Potential Zones

Zone	Area (in sq. km)	Area (in %)
Low	38.11	8.52
Moderate	164.22	36.72
High	244.74	54.75
Total	447.07	100.00

(Source: Calculated by the authors)

Digaru and Kolong rivers tend to overflow during peak monsoon periods, resulting in inundation of adjacent settlements. These zones also exhibit moderate to high drainage density, which contributes to increased flood potential. Analysis of the LULC and NDVI maps indicates that high susceptibility zones are largely associated with anthropogenic land-use patterns, including built-up areas and transportation networks. Monocrop rice cultivation is prevalent in these zones, making agricultural activities more exposed to flood-related impacts.

The moderate and low susceptibility zones are generally located farther from river channels and are associated with relatively elevated terrain and steeper slopes. These zones typically exhibit lower drainage density and denser vegetation cover, which contribute to reduced flood susceptibility. The dominant lithological units in these areas consist mainly of igneous and metamorphic derivatives, which are comparatively less prone to erosion. Population distribution in these zones is relatively moderate and dispersed. Elevated topography remains a key factor contributing to lower flood susceptibility in these areas.

In addition, the spatial configuration of LULC plays an important role in controlling flood susceptibility across Dimoria Block, and spatial analysis reveals patterns consistent with the model output. High susceptibility zones are predominantly associated with agricultural land, settlements, and open areas located along low-lying alluvial plains, where limited infiltration capacity and higher surface runoff contribute to increased flood response [84]. Built-up areas contain extensive impervious surfaces that increase surface runoff and reduce drainage efficiency, explaining their concentration within high susceptibility zones [110]. Moderate susceptibility zones are associated with mixed vegetation, plantations, and sparsely settled areas, where partial land cover and moderately sloping terrain provide some attenuation of runoff [84]. In contrast, low susceptibility zones coincide with forested uplands and areas of dense vegetation, where canopy interception and improved soil permeability enhance infiltration and reduce overland flow accumulation [111]. These spatial relationships reinforce the role of LULC as a significant controlling factor in flood susceptibility and support the model results identifying LULC as one of the dominant parameters in the study area.

While the present study provides a spatial classification of flood susceptibility, it does not include detailed assessments of population exposure, infrastructure distribution, or hydrodynamic parameters such as flood depth or flow velocity. Such analyses require additional socio-economic datasets, river discharge records, and hydraulic modeling frameworks that extend beyond the scope of a GIS–AHP–based susceptibility assessment. The primary objective of this study was to generate a baseline flood hazard zonation map using a multi-criteria evaluation approach. Future studies may integrate exposure analysis and hydrodynamic modeling to improve the quantification of flood impacts and potential economic losses.

7 Validation

The flood susceptibility map is validated integrating the ROC-AUC, primary field survey locations, historical flood records and government reports. The validation has been performed in two ways: quantitatively, the generation of ROC-AUC and qualitatively, comparative analysis with government reports.

The input data for the ROC-AUC validation comprised 150 ground truth points (50% each for both flooded and non-flooded areas) collected during field survey (2024–25) and the GIS generated flood susceptibility map. The locations were chosen based on historical flood maps, flood inundation records of 2020 and flood hazard zonation record [16]. These locations were superimposed on the flood susceptibility map to prepare the ROC-AUC. The efficiency of the model validated by ROC-AUC is classified as poor (0.5–0.6), average (0.6–0.7), good (0.7–0.8), very good (0.8–0.9) and excellent (0.9–1) [85]. The AUC value of our model is 0.936, which stands for 'excellent' [58, 85]. It implies that the model has an excellent prediction ability of flood hazard in the study area. The result confirms the robustness and reliability of the model, which can be applied to similar studies in other geographical contexts (Fig. 15, 16).

Further for qualitative validation, 13 villages from 10 different gaon panchayats have been selected to corroborate the GIS-AHP result with the government reported flood hazard zones (Table 8). Of the 13 assessed villages, only 8 of these villages had

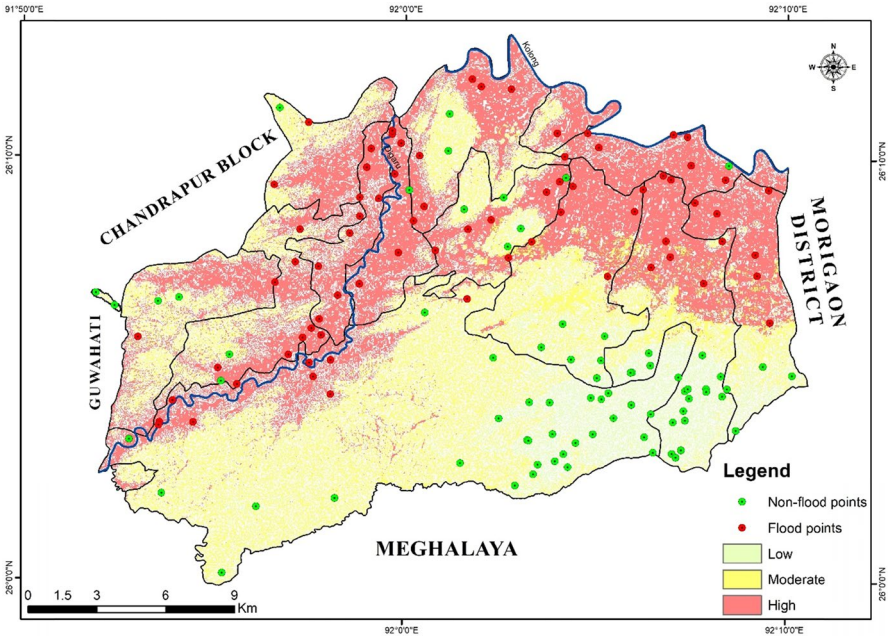

Fig. 15 Random sample points for flood susceptibility map validation in Dimoria Block. 150 ground truth points (50% each for both flooded and non-flooded areas) were collected during field survey (2024–25) and the GIS generated flood susceptibility map. The non-flooded points are represented in green and flooded points in red colors, respectively. The locations were chosen based on historical flood maps, flood inundation records of 2020 and flood hazard zonation record. The points were overlaid on the flood susceptibility map to serve as inputs for the ROC-AUC. The map includes administrative boundaries, drainage lines, neighboring regions, a north arrow, and scale bar

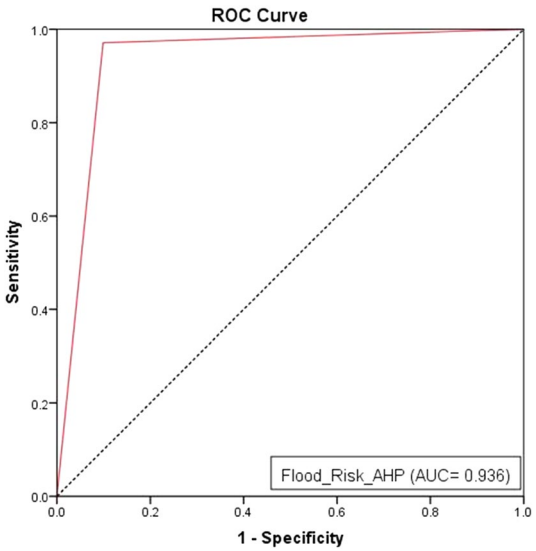

Fig. 16 Receiver Operating Characteristic (ROC) curve for the validation of the GIS–AHP flood-susceptibility model for Dimoria Block. The plot displays model sensitivity (true positive rate) against 1 − specificity (false positive rate) across all decision thresholds; the diagonal line indicates a random classifier for reference. The area under the curve (AUC = 0.936) quantifies overall predictive performance and indicates excellent discrimination between flooded and non-flooded locations. The ROC was derived by comparing the modelled susceptibility classes with independent validation data as described in the Validation procedure (Sect. 7)

Table 8 Location of villages for qualitative validation of GIS output

S.No	Village	Gaon Panchayat	Latitude (°N)	Longitude (°E)	Flood Susceptibility (as per GIS output)	Flood Susceptibility (as per Government Report)
1	Bajeni Gaon	Hahara	26.172	92.006	High	High
2	Barkuchi N.C	Nartap	26.092	91.990	Low	0
3	Dakhin Dimoria (Bahtola)	Dhoupguri	26.092	92.137	Low	0
4	Damara Pathar	Baruabari	26.109	91.976	High	Moderate
5	Dhangiri Gaon	Barkhat	26.140	91.944	Moderate	Moderate
6	Gumoria Pathar	Hahara	26.123	91.962	High	High
7	Hahara Pathar	Hahara	26.160	91.996	High	High
8	Khaloibari Gaon	Khetri	26.108	92.060	Moderate	0
9	Maloibari Gaon	Maloibari	26.176	92.123	High	High
10	Mitani N.C	Tetelia	26.161	92.009	Moderate	Moderate
11	Murkata	Topatoli	26.118	92.143	Moderate	0
12	Sonapur Pathar	Sonapur	26.134	91.999	High	0
13	Tetelia Gaon	Tetelia	26.098	91.987	Moderate	Moderate

(Source: Compiled by the authors based on field survey, 2024–25; 0 = no data available)

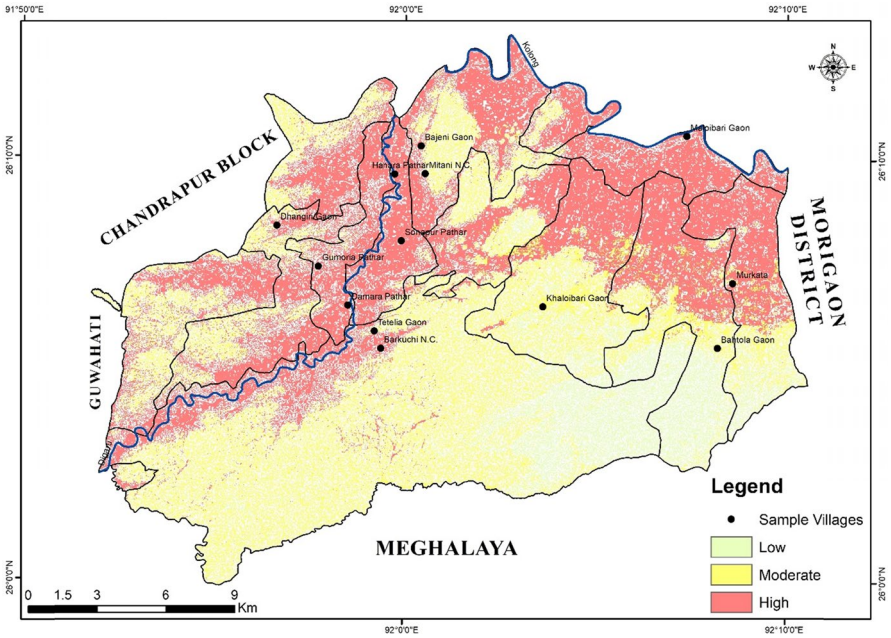

Fig. 17 Location of sample villages for qualitative validation. This map identifies selected villages (highlighted as black points) across Dimoria Block where field verification was conducted to validate the modeled flood susceptibility zones. The locations are plotted over the administrative boundary. A north arrow and scale bar provide spatial reference

corresponding data available in government report for comparison [16]. It was found that 7 of these 8 villages were consistent with the government's findings. Only 1 village

Fig. 18 Field Photographs (2024–25): **a** Flood-affected road in Damara Pathar, **b** Inundated paddy field in Damara Pathar, **c** Waterlogged agricultural land in Hahara Pathar and **d** Elevated water level in the Digaru River near the Sonapur–Byrnihat Road

(Damara Pathar) showed a discrepancy between our results and the official records (Fig. 17).

Bajeni Gaon, Gumoria Pathar, Hahara Pathar, Maloibari Gaon and Sonapur Pathar lie at high susceptibility of flooding. These villages are characterized by a dense human populace, extensive agriculture along with the influence of industrial activities, and a low-lying topography with a few dotted uplands. Maloibari Gaon still comes under the threat of high susceptibility, despite not facing severe floods in recent years because of the embankment along the Kolong river. Dhangiri Gaon, Khaloibari Gaon, Mitani N.C., Murkata and Tetelia Gaon lie at moderate susceptibility whereas Barkuchi N.C. and Dakhin Dimoria (Bahtola Gaon) lie in a low susceptibility zone. The former five villages rarely face frequent flooding, yet episodic rainfall has caused inundation in the past, as stated by the villagers. The latter two villages are least prone to flood because of the elevated topography and dense vegetation cover. The situation of Damara Pathar is unusual since it contradicts the government-published results. Although official records categorize it in the 'moderate' zone, but field visit (Fig. 18 (a) and (b)) and interaction with villagers revealed the frequency and susceptibility associated with floods in the

village. Therefore, the categorization of the village into the 'high' zone by our map seems apt and convincing.

Discrepancies between modelled flood susceptibility zones and government reports often arise because government reports and maps are event-specific and may under-report hazard potential in less populated areas, while models use long-term, multi-factor analysis to identify hazard zones regardless of population [112, 113]. Differences in data years, mapping scales, and missing local drainage details in official records also contribute to mismatches [112]. These differences are common and reflect the gap between actual flood events and broader flood susceptibility, not a flaw in the models [112, 113].

Thus, the GIS generated map adheres to both quantitative and qualitative validation and hence the map can be considered as a fair representation of ground reality.

8 Conclusion

This study presents a comprehensive flood susceptibility assessment of Dimoria Block using an integrated GIS-enabled Analytical Hierarchy Process (AHP) framework. The model effectively delineates three flood susceptibility zones based on eleven flood-conditioning parameters. The results indicate that approximately 54.75% of the study area falls within the high susceptibility zone, while low susceptibility zones account for 8.52% of the total area. High susceptibility zones are primarily associated with low-lying floodplains characterized by gentle terrain, proximity to river channels, and unconsolidated sedimentary formations. In contrast, areas with higher elevation, steeper slopes, and greater distance from river channels correspond to moderate and low susceptibility zones. Validation of the model using predictive accuracy analysis (AUC = 0.936), along with field observations and governmental flood records, demonstrates the robustness of the approach and its applicability for flood hazard management.

The study makes a meaningful contribution by addressing the lack of micro-spatial flood susceptibility assessments in Assam, particularly in semi-urban and rural fringe regions such as Dimoria Block. The analysis identifies rainfall and land use/land cover (LULC) as the most influential parameters, highlighting the combined effects of hydro-climatic variability and anthropogenic land-use modification on flood susceptibility. These findings provide useful insights for disaster risk reduction strategies, including site-specific interventions, improved land-use planning, and informed allocation of mitigation resources.

Despite the effectiveness of the proposed approach, certain limitations should be acknowledged. The use of static spatial datasets limits the representation of temporal dynamics such as seasonal river behavior and long-term climatic variability. Additionally, the model does not incorporate socio-economic vulnerability indicators, which are important for comprehensive assessment of flood impacts. Future research may integrate real-time hydrological data, climate projections, and demographic information to develop more dynamic and inclusive flood risk assessment frameworks.

In summary, the GIS–AHP methodology applied in this study offers a reliable and reproducible tool for flood hazard zonation in data-scarce regions. The approach and findings have practical relevance for local authorities, planners, and disaster management agencies in Northeast India and other flood-prone areas. The study underscores

the role of spatial decision-support systems in enhancing preparedness, supporting informed planning, and promoting sustainable development in hazard-prone regions.

Acknowledgements
The authors would like to acknowledge the BDO Office, Sonapur for providing the block level administrative map which has been used to prepare the base map in the present study. We are also grateful to the people of Dimoria Block for their cooperation and support during the field survey. We acknowledge the kind assistance of Mr. Bhabandao Hojai in the preparation of the flowchart included in this work. Our heartfelt thanks go to the anonymous reviewers for their constructive comments and thoughtful suggestions, which helped improve the quality and clarity of this work.

Author contributions
S.C. conceptualized and wrote the main manuscript text. S.C. performed the analyses and prepared the figures, tables and maps in the manuscript. M.D. reviewed the manuscript and provided suggestions and necessary amendments.

Funding
The authors have no relevant financial or non-financial interests to disclose.

Data availability
The data sources are already provided in the manuscript and are also available upon reasonable request to the corresponding author.

Declarations

Ethics approval and consent to participate
This study involved the analysis of secondary, publicly available geospatial data (DEM, satellite imagery, soil data, etc.) and did not require the use of human subjects, animals, or clinical trials. Therefore, ethical approval from an Institutional Review Board (IRB) or equivalent body was not required.

Consent for publication
The manuscript does not contain any individual person's data in any form.

Competing interests
The authors declare no competing interests.

Use of language editing tools
A language editing tool (ProWritingAid) was used solely to assist with grammar, sentence structure, and clarity of expression. The authors are fully responsible for the scientific content, data analysis, interpretation of results, and conclusions presented in this manuscript.

Received: 23 April 2025 Accepted: 1 March 2026
Published online: 23 March 2026

References

1. Nachappa TG, Piralilou ST, Gholamnia K, Ghorbanzadeh O, Rahmati O, Blaschke T. Flood susceptibility mapping with machine learning, multi-criteria decision analysis and ensemble using Dempster Shafer Theory. J Hydrol. 2020;590:125275. https://doi.org/10.1016/j.jhydrol.2020.125275.
2. Van CT, Tri DQ, Son NT, Thao TTT, Hoa DTH. Determining the vulnerability index in the context of high floods in An Giang province. IOP Conf Ser Earth Environ Sci. 2019;307(1):012015. https://doi.org/10.1088/1755-1315/307/1/012015.
3. Igibah EC, Sadiq AA. Impact of flood danger in built-up areas in Nigeria and floor management systems for espousal. IOP Conf Ser Mater Sci Eng. 2018;413:012033. https://doi.org/10.1088/1757-899x/413/1/012033.
4. Tingsanchali T. Urban flood disaster management. Procedia Eng. 2012;32:25–37. https://doi.org/10.1016/j.proeng.2012.01.1233.
5. Aznar-Crespo P, Aledo A, Melgarejo-Moreno J, Vallejos-Romero A. Adapting social impact assessment to flood risk management. Sustainability. 2021;13(6):3410. https://doi.org/10.3390/su13063410.
6. Maher, B., Million, N., & International Monetary Fund. (2024). FLOOD EVENTS OF 2023–2024. In *INTERNATIONAL MONETARY FUND* (pp. 65–68).
7. *FACT BOX - Major floods in South Asia since 2020*. (2025, July 18). Retrieved July 20, 2025, from https://www.aa.com.tr/en/asia-pacific/fact-box-major-floods-in-south-asia-since-2020/3635170
8. Tempa K. District flood vulnerability assessment using analytic hierarchy process (AHP) with historical flood events in Bhutan. PLoS ONE. 2022;17(6):e0270467. https://doi.org/10.1371/journal.pone.0270467.
9. Yusmah MYS, Bracken LJ, Sahdan Z, Norhaslina H, Melasutra MD, Ghaffarianhoseini A, et al. Understanding urban flood vulnerability and resilience: a case study of Kuantan, Pahang, Malaysia. Nat Hazards. 2020;101(2):551–71. https://doi.org/10.1007/s11069-020-03885-1.
10. Ashraf S, Luqman M, Iftikhar M, Ashraf I, Hassan ZY. Understanding Flood risk management in Asia: Concepts and challenges. In InTech eBooks. 2017. https://doi.org/10.5772/intechopen.69139.
11. Mohanty MP, Mudgil S, Karmakar S. Flood management in India: a focussed review on the current status and future challenges. Int J Disaster Risk Reduct. 2020;49:101660. https://doi.org/10.1016/j.ijdrr.2020.101660.

12. Borah, S., & Buragohain, A. (2023). Assam Flood and Financial loss in Agricultural Production: A study on mitigation strategy adopted by the farmers of Dhemaji District. *Agricultural Reviews*, *Of*. https://doi.org/10.18805/ag.r-2625
13. Gupta L, Dixit J. A GIS-based flood risk mapping of Assam, India, using the MCDA-AHP approach at the regional and administrative level. Geocarto Int. 2022;37(26):11867–99. https://doi.org/10.1080/10106049.2022.2060329.
14. S, S. S., V., Roy, P. S., V, C., & G, S. R. (2017). Flood risk assessment using multi-criteria analysis: a case study from Kopili River Basin, Assam, India. *Geomatics Natural Hazards and Risk*, *9*(1), 79–93. https://doi.org/10.1080/19475705.2017.1408705
15. Hirabayashi Y, Mahendran R, Koirala S, Konoshima L, Yamazaki D, Watanabe S, et al. Global flood risk under climate change. Nat Clim Chang. 2013;3(9):816–21. https://doi.org/10.1038/nclimate1911.
16. Flood Hazard Zonation Atlas of Assam - using multi-sensor satellite data (1998–2023). (2025). In *NRSC* (Version-3.0). NRSC and ISRO. Retrieved July 18, 2025, from https://www.nrsc.gov.in
17. Das I, Deka S. Impact of flood on the socio-economic conditions in the southern part of Kamrup district, Assam. Space Cult India. 2021;8(4):106–19. https://doi.org/10.20896/saci.v8i4.665.
18. GOVERNMENT OF ASSAM. (n.d.). FLOOD MEMORANDUM. In *TO THE MINISTRY OF HOME AFFAIRS GOVERNMENT OF INDIA ON ASSAM FLOODS –2024* (p. 3).
19. Cislaghi, A., & Bischetti, G. B. (2022). Best practices in post-flood surveys: The study case of Pioverna torrent. *Journal of Agricultural Engineering*, *53*(2). https://doi.org/10.4081/jae.2022.1312
20. Mathew AE, Kumar SS, Vivek G, Iyyappan M, Karthikaa R, Kumar PD, et al. Flood impact assessment using field investigations and post-flood survey. J Earth Syst Sci. 2021. https://doi.org/10.1007/s12040-021-01657-4.
21. González-Cao J, Barreiro-Fonta H, Fernández-Nóvoa D, García-Feal O. Enhancing Flood Risk Management: A review on numerical modelling of past flood events. Hydrology. 2025;12(6):133. https://doi.org/10.3390/hydrology12060133.
22. Irimescu, A., Stancalie, G., Craciunescu, V., Flueraru, C., & Anderson, E. (2009). The use of remote sensing and GIS techniques in flood monitoring and damage assessment: a study case in Romania. In *NATO science for peace and security series. C, Environmental security* (pp. 167–177). https://doi.org/10.1007/978-90-481-2344-5_18
23. Jeyaseelan, A. T., National Remote Sensing Agency, & Department of Space, Govt. of India, Hyderabad. (n.d.). DROUGHTS & FLOODS ASSESSMENT AND MONITORING USING REMOTE SENSING AND GIS. In *Satellite Remote Sensing and GIS Applications in Agricultural Meteorology* (pp. 291–313).
24. Dasgupta, A., Grimaldi, S., Ramsankaran, R., Pauwels, V. R. N., Walker, J. P., Chini, M., Hostache, R., & Matgen, P. (2018). Flood mapping using synthetic aperture radar sensors from local to global scales. *Geophysical Monograph*, 55–77. https://doi.org/10.1002/9781119217886.ch4
25. Lang F, Zhu Y, Zhao J, Hu X, Shi H, Zheng N, et al. Flood mapping of Synthetic Aperture Radar (SAR) imagery based on Semi-Automatic Thresholding and Change Detection. Remote Sensing. 2024;16(15):2763. https://doi.org/10.3390/rs16152763.
26. Essahlaoui, N., Ijlil, S., Alitane, A., Mohajane, M., Ouali, A. E., Rhazi, A., Oumou, A., Alouane, A., Ammari, Z., Khrabcha, A., Hafyani, M. E., Essahlaoui, A., Aouragh, M. H., & Van Rompaey, A. (2025). Using GIS and Analytical Hierarchy Process (AHP) for flood hazard assessment based on morphological and hydrological criteria, case of the Meknes region, Morocco. *E3S Web of Conferences*, *607*, 04009. https://doi.org/10.1051/e3sconf/202560704009
27. Mokhtari E, Mezali F, Abdelkebir B, Engel B. Flood risk assessment using analytical hierarchy process: a case study from the Cheliff-Ghrib watershed, Algeria. J Water Clim Change. 2023;14(3):694–711. https://doi.org/10.2166/wcc.2023.316.
28. Mitra R, Saha P, Das J. Assessment of the performance of GIS-based analytical hierarchical process (AHP) approach for flood modelling in Uttar Dinajpur district of West Bengal. India Geomatics Natural Hazards and Risk. 2022;13(1):2183–226. https://doi.org/10.1080/19475705.2022.2112094.
29. Kouamé PK, Fokou G, Koffi AJD, Sani A, Bonfoh B, Dongo K. Assessing institutional stakeholders' perception and limitations on coping strategies in flooding risk management in West Africa. Int J Environ Res Public Health. 2022;19(11):6933. https://doi.org/10.3390/ijerph19116933.
30. Mourato S, Fernandez P, Pereira LG, Moreira M. Assessing vulnerability in flood prone areas using Analytic Hierarchy Process—Group Decision Making and Geographic Information System: a case study in Portugal. Appl Sci. 2023;13(8):4915. https://doi.org/10.3390/app13084915.
31. AlAli AM, Salih A, Hassaballa A. Geospatial-Based Analytical Hierarchy Process (AHP) and Weighted Product Model (WPM) techniques for mapping and assessing flood susceptibility in the Wadi Hanifah Drainage Basin, Riyadh region. Saudi Arabia Water. 2023;15(10):1943. https://doi.org/10.3390/w15101943.
32. Chen Y. Application of Analytic Hierarchy Process (AHP) and simple additive weighting (SAW) methods in mapping Flood-Prone areas. In Frontiers in artificial intelligence and applications. 2021. https://doi.org/10.3233/faia210274.
33. Assam: Boy swept away by floodwaters in Dimoria, 40,000 hit in Sonapur circle. (2019, July 18). *The Times of India*. Retrieved July 18, 2025, from https://timesofindia.indiatimes.com/city/guwahati/assam-boy-swept-away-by-floodwaters-in-dimoria-40000-hit-in-sonapur-circle/articleshow/70271113.cms
34. Team NERDRR. (2020). *Flood scenario of Assam as on 28th May 2020*.
35. Team NERDRR. (2020). *Flood scenario of Assam as on 24th June 2020*.
36. DRIMS Assam. (n.d.). Assam Flood Report As on 15–07–2024. In *DRIMS Assam*.
37. Deka, D. R. (2020). A study on morphological pattern and degradation of wetlands in Dimoria, Assam. In Sonapur College, *Journal of Emerging Technologies and Innovative Research* (Vol. 7, Issue 11). https://www.jetir.org
38. De Brito MM, Evers M. Multi-criteria decision-making for flood risk management: a survey of the current state of the art. Nat Hazards Earth Syst Sci. 2016;16(4):1019–33. https://doi.org/10.5194/nhess-16-1019-2016.
39. Siam ZS, Hasan RT, Anik SS, Noor F, Adnan MSG, Rahman RM, et al. National-scale flood risk assessment using GIS and remote sensing-based hybridized deep neural network and fuzzy analytic hierarchy process models: a case of Bangladesh. Geocarto Int. 2022;37(26):12119–48. https://doi.org/10.1080/10106049.2022.2063411.
40. Radwan F, Alazba AA, Mossad A. Flood risk assessment and mapping using AHP in arid and semiarid regions. Acta Geophys. 2018;67(1):215–29. https://doi.org/10.1007/s11600-018-0233-z.

41. Lin L, Wu Z, Liang Q. Urban flood susceptibility analysis using a GIS-based multi-criteria analysis framework. Nat Hazards. 2019;97(2):455–75. https://doi.org/10.1007/s11069-019-03615-2.
42. Tariq A, Yan J, Ghaffar B, Qin S, Mousa BG, Sharifi A, et al. Flash flood susceptibility assessment and zonation by integrating analytic hierarchy process and frequency ratio model with diverse spatial data. Water. 2022;14(19):3069. https://doi.org/10.3390/w14193069.
43. Ali SA, Khatun R, Ahmad A, Ahmad SN. Application of GIS-based analytic hierarchy process and frequency ratio model to flood vulnerable mapping and risk area estimation at Sundarban region, India. Model Earth Syst Environ. 2019;5(3):1083–102. https://doi.org/10.1007/s40808-019-00593-z.
44. Debnath J, Sahariah D, Mazumdar M, Lahon D, Meraj G, Hashimoto S, et al. Evaluating flood susceptibility in the Brahmaputra River Basin: an insight into Asia's Eastern Himalayan Floodplains using machine learning and multi-criteria decision-making. Earth Syst Environ. 2023;7(4):733–60. https://doi.org/10.1007/s41748-023-00358-w.
45. Das S. Flood susceptibility mapping of the Western Ghat coastal belt using multi-source geospatial data and analytical hierarchy process (AHP). Remote Sens Appl Soc Environ. 2020;20:100379. https://doi.org/10.1016/j.rsase.2020.100379.
46. Bhuyan MJ, Deka N, Saikia A. Micro-spatial flood risk assessment in Nagaon district, Assam (India) using GIS-based multi-criteria decision analysis (MCDA) and analytical hierarchy process (AHP). Risk Anal. 2023;44(4):817–32. https://doi.org/10.1111/risa.14191.
47. Borah PB, Handique A, Dutta CK, Bori D, Acharjee S, Longkumer L. Assessment of flood susceptibility in Cachar district of Assam, India using GIS-based multi-criteria decision-making and analytical hierarchy process. Nat Hazards. 2025. https://doi.org/10.1007/s11069-024-07100-3.
48. De Brito MM, Almoradie A, Evers M. Spatially-explicit sensitivity and uncertainty analysis in a MCDA-based flood vulnerability model. Int J Geogr Inf Sci. 2019;33(9):1788–806. https://doi.org/10.1080/13658816.2019.1599125.
49. Mitra R, Das J. A comparative assessment of flood susceptibility modelling of GIS-based TOPSIS, VIKOR, and EDAS techniques in the Sub-Himalayan foothills region of Eastern India. Environ Sci Pollut Res. 2022;30(6):16036–67. https://doi.org/10.1007/s11356-022-23168-5.
50. Senan CPC, Ajin RS, Danumah JH, Costache R, Arabameri A, Rajaneesh A, et al. Flood vulnerability of a few areas in the foothills of the Western Ghats: a comparison of AHP and F-AHP models. Stoch Env Res Risk Assess. 2022;37(2):527–56. https://doi.org/10.1007/s00477-022-02267-2.
51. Amiri A, Soltani K, Ebtehaj I, Bonakdari H. A novel machine learning tool for current and future flood susceptibility mapping by integrating remote sensing and geographic information systems. J Hydrol. 2024;632:130936. https://doi.org/10.1016/j.jhydrol.2024.130936.
52. Sahraei R, Kanani-Sadat Y, Homayouni S, Safari A, Oubennaceur K, Chokmani K. A novel hybrid GIS -based multi-criteria decision-making approach for flood susceptibility analysis in large ungauged watersheds. J Flood Risk Manag. 2022. https://doi.org/10.1111/jfr3.12879.
53. District Census Handbook Kamrup Metropolitan, Village and Town Directory. (2011). In *Kamrup Metropolitan District* (Part XII-A, Series-19). DIRECTORATE OF CENSUS OPERATIONS, ASSAM. https://share.google/w154ruVVlcOTqDfs2
54. Costache R, Pham QB, Sharifi E, Linh NTT, Abba S, Vojtek M, et al. Flash-flood susceptibility assessment using multi-criteria decision making and machine learning supported by remote sensing and GIS techniques. Remote Sensing. 2019;12(1):106. https://doi.org/10.3390/rs12010106.
55. Mokhtari E, Abdelkebir B, Djenaoui A, Hamdani NEH. Integrated analytic hierarchy process and fuzzy analytic hierarchy process for Sahel watershed flood susceptibility assessment, Algeria. Water Practice & Technology. 2024;19(2):453–75. https://doi.org/10.2166/wpt.2024.012.
56. Ahmed IA, Talukdar S, Shahfahad N, Parvez A, Rihan M, Baig MRI, et al. Flood susceptibility modeling in the urban watershed of Guwahati using improved metaheuristic-based ensemble machine learning algorithms. Geocarto Int. 2022;37(26):12238–66. https://doi.org/10.1080/10106049.2022.2066200.
57. Singha C, Swain KC, Meliho M, Abdo HG, Almohamad H, Al-Mutiry M. Spatial analysis of flood hazard zoning map using novel hybrid machine learning technique in Assam, India. Remote Sensing. 2022;14(24):6229. https://doi.org/10.3390/rs14246229.
58. Ahmed I, Das N, Debnath J, Bhowmik M, Bhattacharjee S. Flood hazard zonation using GIS-based multi-parametric analytical hierarchy process. Geosystems and Geoenvironment. 2023;3(2):100250. https://doi.org/10.1016/j.geogeo.2023.100250.
59. Samanta RK, Bhunia GS, Shit PK, Pourghasemi HR. Flood susceptibility mapping using geospatial frequency ratio technique: a case study of Subarnarekha River Basin, India. Modeling Earth Systems and Environment. 2018;4(1):395–408. https://doi.org/10.1007/s40808-018-0427-z.
60. Shrestha S, Dahal D, Poudel B, Banjara M, Kalra A. Flood susceptibility analysis with integrated geographic information system and analytical hierarchy process: a multi-criteria framework for risk assessment and mitigation. Water. 2025;17(7):937. https://doi.org/10.3390/w17070937.
61. Vojtek M, Vojteková J. Flood susceptibility mapping on a national scale in Slovakia using the Analytical Hierarchy Process. Water. 2019;11(2):364. https://doi.org/10.3390/w11020364.
62. Stambaugh MC, Guyette RP. Predicting spatio-temporal variability in fire return intervals using a topographic roughness index. For Ecol Manage. 2007;254(3):463–73. https://doi.org/10.1016/j.foreco.2007.08.029.
63. Bordoloi, B., Bora, K., Choudhury, S., Sonowal, K., Sahu, S., Hazarika, D., & Deka, P. (2024). Flood hazard mapping and monitoring in the Kamrup district of the Lower Brahmaputra Valley, Assam: A geospatial appraisal. In *Springer natural hazards* (pp. 375–400). https://doi.org/10.1007/978-981-97-2688-2_18
64. Robinson N, Allred B, Jones M, Moreno A, Kimball J, Naugle D, et al. A dynamic Landsat derived Normalized Difference Vegetation Index (NDVI) product for the conterminous United States. Remote Sens. 2017;9(8):863. https://doi.org/10.3390/rs9080863.
65. Choudhury, S., & Garg, B. (2021). Groundwater Potential Mapping of East Guwahati: A Geospatial study. In *Sustainable approach to resource management for social development*. Assam Book Hive.

66. Chen, J., Yang, S. T., Li, H. W., Zhang, B., & Lv, J. R. (2013). Research on Geographical Environment Unit Division based on the Method of Natural Breaks (JENKs). *The International Archives of the Photogrammetry, Remote Sensing and Spatial Information Sciences/International Archives of the Photogrammetry, Remote Sensing and Spatial Information Sciences*, *XL-4/W3*, 47–50. https://doi.org/10.5194/isprsarchives-xl-4-w3-47-2013
67. Dutta M, Choudhury S. Crop productivity zones in Assam: a geospatial analysis. North-East Geogr. 2023;42(1 and 2):0973–915.
68. Jenks GF. The data model concept in statistical mapping. Int Yearb Cartogr. 1967;7:186–90.
69. Esri: GIS Software for Mapping and Spatial Analytics. (2022). ESRI. https://www.esri.com/en-us/home
70. Malczewski JA. GIS and Multi Criteria Decision Analysis. New York: John Wiley & Sons; 1999. p. 392.
71. Saha A, Pal S, Arabameri A, Blaschke T, Panahi S, Chowdhuri I, et al. Flood susceptibility assessment using novel ensemble of hyperpipes and support vector regression algorithms. Water. 2021;13(2):241. https://doi.org/10.3390/w13020241.
72. Amen ARM, Mustafa A, Kareem DA, Hameed HM, Mirza AA, Szydłowski M, et al. Mapping of flood-prone areas utilizing GIS techniques and remote sensing: A case study of Duhok, Kurdistan Region of Iraq. Remote Sens. 2023;15(4):1102. https://doi.org/10.3390/rs15041102.
73. M S, Nanda S. Futuristic flood risks assessment, in the Upper Vellar Basin, integrating AHP and bivariate analysis. Adv Space Res. 2024;74(11):5395–416. https://doi.org/10.1016/j.asr.2024.08.030.
74. Singha C, Sahoo S, Mahtaj AB, Moghimi A, Welzel M, Govind A. Advancing flood risk assessment: multitemporal SAR-based flood inventory generation using transfer learning and hybrid fuzzy-AHP-machine learning for flood susceptibility mapping in the Mahananda River Basin. J Environ Manage. 2025;380:124972. https://doi.org/10.1016/j.jenvman.2025.124972.
75. Allafta H, Opp C. GIS-based multi-criteria analysis for flood prone areas mapping in the trans-boundary Shatt Al-Arab Basin, Iraq-Iran. Geomat Nat Hazards Risk. 2021;12(1):2087–116. https://doi.org/10.1080/19475705.2021.1955755.
76. Jodhani KH, Patel D, Madhavan N, Gupta N, Singh SK, Rathnayake U. Unravelling flood risk in the Rel River Watershed, Gujarat using coupled earth observations, multi criteria decision making and Google Earth Engine. Results Eng. 2024;24:102836. https://doi.org/10.1016/j.rineng.2024.102836.
77. Sonowal, K., & Choudhury, S. (2023). *ANWESHAN: A collection of articles* (1st ed.). J S Publications.
78. Saaty TL. Decision making with the analytic hierarchy process. Int J Serv Sci. 2008;1(1):83. https://doi.org/10.1504/ijssci.2008.017590.
79. Mukherjee I, Singh UK. Delineation of groundwater potential zones in a drought-prone semi-arid region of East India using GIS and analytical hierarchical process techniques. CATENA. 2020;194:104681. https://doi.org/10.1016/j.catena.2020.104681.
80. Verma N, Patel RK. Delineation of groundwater potential zones in Lower Rihand River Basin, India using geospatial techniques and AHP. Egypt J Remote Sens Space Sci. 2021;24(3):559–70. https://doi.org/10.1016/j.ejrs.2021.03.005.
81. Fenta AA, Kifle A, Gebreyohannes T, Hailu G. Spatial analysis of groundwater potential using remote sensing and GIS-based multi-criteria evaluation in Raya Valley, Northern Ethiopia. Hydrogeol J. 2014;23(1):195–206. https://doi.org/10.1007/s10040-014-1198-x.
82. Lodwick WA, Monson W, Svoboda L. Attribute error and sensitivity analysis of map operations in geographical informations systems: suitability analysis. Int J Geogr Inf Syst. 1990;4(4):413–28. https://doi.org/10.1080/02693799008941556.
83. Kindie, A. T., Enku, T., Moges, M. A., Geremew, B. S., & Atinkut, H. B. (2019). Spatial analysis of groundwater potential using GIS based multi criteria decision analysis method in Lake Tana Basin, Ethiopia. In *Springer eBooks* (pp. 439–456). https://doi.org/10.1007/978-3-030-15357-1_37
84. Ashfaq S, Tufail M, Niaz A, Muhammad S, Alzahrani H, Tariq A. Flood susceptibility assessment and mapping using GIS-based analytical hierarchy process and frequency ratio models. Glob Planet Change. 2025. https://doi.org/10.1016/j.gloplacha.2025.104831.
85. Rana SS, Habib SA, Sharifee MNH, Sultana N, Rahman SH. Flood risk mapping of the flood-prone Rangpur division of Bangladesh using remote sensing and multi-criteria analysis. Nat Hazards Res. 2023;4(1):20–31. https://doi.org/10.1016/j.nhres.2023.09.012.
86. Swets JA. Measuring the accuracy of diagnostic systems. Science. 1988;240(4857):1285–93. https://doi.org/10.1126/science.3287615.
87. Çellek S. Effect of the slope angle and its classification on landslide. 2020. Nat Hazards Earth Syst Sci. https://doi.org/10.5194/nhess-2020-87.
88. Jing X, Chen Y, Pan C, Yin T, Wang W, Fan X. Erosion failure of a soil slope by heavy rain: laboratory investigation and modified GA model of soil slope failure. Int J Environ Res Public Health. 2019;16(6):1075. https://doi.org/10.3390/ijerph16061075.
89. Desalegn H, Mulu A. Flood vulnerability assessment using GIS at Fetam Watershed, upper Abbay Basin, Ethiopia. Heliyon. 2021;7(1):e05865. https://doi.org/10.1016/j.heliyon.2020.e05865.
90. Rincón D, Khan UT, Armenakis C. Flood risk mapping using GIS and multi-criteria analysis: A Greater Toronto Area case study. Geosciences. 2018;8(8):275. https://doi.org/10.3390/geosciences8080275.
91. Ntanganedzeni B, Nobert J. Flood risk assessment in Luvuvhu River, Limpopo Province, South Africa. Physics and Chemistry of the Earth Parts a/B/C. 2020;124:102959. https://doi.org/10.1016/j.pce.2020.102959.
92. Rezende OM, Da Cruz De Franco ABR, De Oliveira AKB, Miranda FM, Jacob ACP, De Sousa MM, et al. Mapping the flood risk to socioeconomic recovery capacity through a multicriteria index. J Clean Prod. 2020;255:120251. https://doi.org/10.1016/j.jclepro.2020.120251.
93. Xu C, Fu H, Yang J, Wang L. Assessment of the relationship between land use and flood risk based on a coupled hydrological–hydraulic model: A case study of Zhaojue River Basin in Southwestern China. Land. 2022;11(8):1182. https://doi.org/10.3390/land11081182.

94. Xing Y, Shao D, Ma X, Zhang S, Jiang G. Investigation of the importance of different factors of flood inundation modeling applied in urbanized area with variance-based global sensitivity analysis. The Science of the Total Environment. 2021;772:145327. https://doi.org/10.1016/j.scitotenv.2021.145327.
95. Xue J, Su B. Significant remote sensing vegetation indices: A review of developments and applications. Journal of Sensors. 2017;2017:1–17. https://doi.org/10.1155/2017/1353691.
96. Sindhu D, Sadashivappa N, Ravikumar A, Shivakumar B. Quantitative analysis of catchment using remote sensing and geographic information system. Aquatic Procedia. 2015;4:1421–8. https://doi.org/10.1016/j.aqpro.2015.02.184.
97. Simanton NJR, Hawkins NRH, Mohseni-Saravi NM, Renard NKG. Runoff curve number variation with drainage area, Walnut Gulch, Arizona. Trans ASAE. 1996;39(4):1391–4. https://doi.org/10.13031/2013.27630.
98. Avand M, Moradi HR, Lasboyee MR. Spatial prediction of future flood risk: An approach to the effects of climate change. Geosciences. 2021;11(1):25. https://doi.org/10.3390/geosciences11010025.
99. Annis A, Nardi F, Petroselli A, Apollonio C, Arcangeletti E, Tauro F, et al. UAV-DEMs for small-scale flood hazard mapping. Water. 2020;12(6):1717. https://doi.org/10.3390/w12061717.
100. Sarkar SK, Ansar SB, Ekram KMM, Khan MH, Talukdar S, Naikoo MW, et al. Developing robust flood susceptibility model with small numbers of parameters in highly fertile regions of Northwest Bangladesh for sustainable flood and agriculture management. Sustainability. 2022;14(7):3982. https://doi.org/10.3390/su14073982.
101. Al-Kindi KM, Alabri Z. Investigating the role of the key conditioning factors in flood susceptibility mapping through machine learning approaches. Earth Syst Environ. 2024;8(1):63–81. https://doi.org/10.1007/s41748-023-00369-7.
102. Twumasi YA, Merem EC, Namwamba JB, Okwemba R, Ayala-Silva T, Abdollahi K, et al. Use of GIS and remote sensing technology as a decision support tool in flood disaster management: the case of Southeast Louisiana, USA. J Geogr Inf Syst. 2020;12(02):141–57. https://doi.org/10.4236/jgis.2020.122009.
103. Munyai, R. B., Musyoki, A., & Nethengwe, N. S. (2019). An assessment of flood vulnerability and adaptation: A case study of Hamutsha-Muungamunwe village, Makhado municipality. *Jàmbá Journal of Disaster Risk Studies*, *11*(2). https://doi.org/10.4102/jamba.v11i2.692
104. Mouri G, Shiiba M, Hori T, Oki T. Modeling reservoir sedimentation associated with an extreme flood and sediment flux in a mountainous granitoid catchment, Japan. Geomorphology. 2010;125(2):263–70. https://doi.org/10.1016/j.geomorph.2010.09.026.
105. J, O. O. (2012). Depositional Environments and Petrographic Characteristics of Bida Formation around Share-Pategi, Northern Bida Basin, Nigeria. *Journal of Geography and Geology*, *4*(1). https://doi.org/10.5539/jgg.v4n1p224
106. Nsor M, Akpan A. Characterization and land suitability evaluation for cocoyam in Southern Nigeria. Ghana J Agric Sci. 2021;56(1):26–47. https://doi.org/10.4314/gjas.v56i1.3.
107. Sánchez-Rodríguez AR, Hill PW, Chadwick DR, Jones DL. Crop residues exacerbate the negative effects of extreme flooding on soil quality. Biol Fertil Soils. 2017;53(7):751–65. https://doi.org/10.1007/s00374-017-1214-0.
108. Yonaba R, Biaou AC, Koïta M, Tazen F, Mounirou LA, Zouré CO, et al. A dynamic land use/land cover input helps in picturing the Sahelian paradox: assessing variability and attribution of changes in surface runoff in a Sahelian watershed. Sci Total Environ. 2020;757:143792. https://doi.org/10.1016/j.scitotenv.2020.143792.
109. Bahddou S, Otten W, Whalley WR, Shin H, Gharous ME, Rickson RJ. Changes in soil surface properties under simulated rainfall and the effect of surface roughness on runoff, infiltration and soil loss. Geoderma. 2023;431:116341. https://doi.org/10.1016/j.geoderma.2023.116341.
110. Feng B, Zhang Y, Bourke R. Urbanization impacts on flood risks based on urban growth data and coupled flood models. Nat Hazards. 2021;106(1):613–27. https://doi.org/10.1007/s11069-020-04480-0.
111. Bradshaw CJA, Sodhi NS, Peh KS, Brook BW. Global evidence that deforestation amplifies flood risk and severity in the developing world. Glob Chang Biol. 2007;13(11):2379–95. https://doi.org/10.1111/j.1365-2486.2007.01446.x.
112. Pralle S. Drawing lines: FEMA and the politics of mapping flood zones. Clim Change. 2018;152(2):227–37. https://doi.org/10.1007/s10584-018-2287-y.
113. Flores AB, Collins TW, Grineski SE, Amodeo M, Porter JR, Sampson CC, et al. Federally overlooked flood risk inequities in Houston, Texas: novel insights based on dasymetric mapping and state-of-the-art flood modeling. Ann Am Assoc Geogr. 2022;113(1):240–60. https://doi.org/10.1080/24694452.2022.2085656.

Publisher's Note